Cortico-striatal action control inherent of opponent cognitive-motivational styles

Cassandra Avila[1] and Martin Sarter[1,2*]

[1]Department of Psychology, University of Michigan, Ann Arbor, MI, USA; [2]Department of Psychology & Neuroscience Program, University of Michigan, Ann Arbor, MI, USA

Running title: Striatal glutamate as a function of attentional bias

Author contributions: CA conducted all the experiments and data analyses. CA and MS designed the experiments and wrote the paper.

***Corresponding author:** Martin Sarter, University of Michigan, Dept. of Psychology, 530 Church Street, Ann Arbor, MI 48109; phone: 734-764-6392; email: msarter@umich.edu.

Number of Figures: 8
Number of Tables: 1
Number of Multimedia: 0
Number of words for Abstract: 250
Number of words for Significance Statement: 110
Number of words for Introduction: 749
Number of words for Discussion: 1,500

Conflict of Interest: Authors report no conflict of interest.

Funding source: The research described in this manuscript was supported by PHS grants R01DA045063 (MS) and P50NS091856 (Morris K. Udall Center for 21 Excellence in Parkinson's Disease Research).

Acknowledgment: We thank Dr. Emma Reznick (University of Michigan) for assistance with the analysis of amperometry data.

Abstract

Turning on cue or stopping at a red light requires the detection of such cues to select action sequences, or suppress action, in accordance with cue-associated action rules. Cortico-striatal projections are an essential part of the brain's attention-motor interface. Here, we used glutamate-sensing microelectrode arrays to measure glutamate transients in the dorsomedial striatum (DMS) of male and female rats walking a treadmill and executing cued turns and stops. Prelimbic-DMS projections were chemogenetically inhibited to determine their behavioral necessity and the cortico-striatal origin of cue-evoked glutamate transients. Furthermore, we investigated rats exhibiting preferably goal-directed (goal trackers, GTs) versus cue-driven attention (sign trackers, STs), to determine the impact of such cognitive-motivational biases on cortico-striatal control. GTs executed more cued turns, and initiated such turns more slowly, than STs. During turns, but not missed turns or cued stops, cue-evoked glutamate concentrations were higher in GTs than in STs. In conjunction with turn cue-evoked glutamate spike levels, the presence of a single spike rendered GTs to be almost twice as likely to turn than STs. In contrast, multiple glutamate spikes predicted STs to be robustly more likely to turn than GTs. In GTs, inhibition of prelimbic-DMS projections attenuated turn rates and turn cue-evoked glutamate peaks and increased the number of spikes. These findings suggest that turn cue-evoked glutamate release dynamics in GTs are tightly controlled by cortico-striatal neuronal activity. In contrast, in STs, glutamate release from DMS glutamatergic terminals is regulated by other striatal circuitry, preferably mediating cued suppression of action and reward tracking.

Significance Statement

Adaptive behavior involves the selection of behaviorally significant cues and the capacity of selected cues to control behavioral action. Neuronal projections from cortex to striatum are essential for such an integration of attentional with motor functions. Here we demonstrated that glutamate release from cortico-striatal projections primarily influences cued turns but not cued suppression of actions (cued stops). Cortico-striatal control of cued turning was especially powerful in rats which, as a psychological trait, preferably deploy goal-directed attention. Together, our findings demonstrate the role of cortico-striatal input in cued action selection, and they emphasize the experimental and biopsychological significance of investigating the brain's attentional-motor interface in the context of broader cognitive-motivational styles.

Key words:

cortex; striatum; glutamate; cued movement control; acetylcholine; attention; substance use disorder; Parkinson's Disease.

Introduction

Cue-triggered selection of action, or suppression of action, are essential components of adaptive behavior. Fronto-striatal projections “import” information about attended cues into the striatum to prioritize cue-linked action, and to facilitate modification of action selection in response to changing action outcomes (Balleine and O'Doherty, 2010; van Schouwenburg et al., 2012; Chatham et al., 2014; Hart et al., 2018a; Hart et al., 2018b). Deficient or biased cortico-striatal cue import has been postulated to cause neuro-psychiatric symptoms ranging from complex movement control deficits in Parkinson’s Disease (PD) to compulsive addictive drug use (Volkow et al., 2006; Bohnen et al., 2009; Ersche et al., 2011; Marshall and Ostlund, 2018; Rasooli et al., 2021; Sarter et al., 2021).

The cortical control of striatal action selection has been extensively supported by studies investigating the effects of manipulation of the excitability of fronto-striatal neurons in non-human animals (for review see Sharpe et al., 2019), and fronto-cortical functional connectivity in humans (Postuma and Dagher, 2006; Shepherd, 2013; Devignes et al., 2022). The present experiments were designed to directly determine the fronto-striatal representation of action-initiating and action-suppressing movement cues. Focusing on the prelimbic projections to DMS (Mailly et al., 2013), that previously were demonstrated to be necessary for learning goal-directed actions (Hart et al., 2018b; Choi et al., 2023), we measured real-time cue-locked glutamate release in the DMS, using amperometry and glutamate-sensing electrodes, and inhibited prelimbic-DMS projections to attribute such release to activity in this pathway.

Glutamate transients were recorded in rats performing visual and auditory cue-triggered turns and stops while walking a treadmill that was stopped and restarted in reverse or same direction, respectively. The development of this task, the Cued-Triggered Turning Task (CTTT; Avila et al., 2020), was inspired by evidence showing that PD fallers exhibited deficient turns (Stack and Ashburn, 2008; Cheng et al., 2014). In PD patients, the propensity for falls has been attributed to loss of cholinergic neurons innervating cortical areas and the resulting failure to select and evaluate movement cues (Bohnen et al., 2009; Yarnall et al., 2011; Rochester et al., 2012; Bohnen et al., 2019; Kim et al., 2019; Sarter et al., 2021). Supporting the validity of the CTTT, in terms of revealing clinically relevant, attentional-motor deficiencies, rats modeling PD falls (Kucinski et al., 2013; Sarter et al., 2014; Kucinski et al., 2015) were demonstrated to exhibit deficits in cued turning, but not cued stopping (Avila et al., 2020).

Performing well-practiced, visually or auditorily cued turns and cued stops requires sustaining attention to cue sources the continued selection of cues as signified by cue-triggered behavior (termed cue detection; Posner et al., 1980), monitoring the state of the treadmill and action outcome, and maintaining cue modality-linked rules in working memory. Cortico-striatal control of action selection was expected to reflect the capacity for such voluntary, or top-down, attentional control.

To reveal the impact of variations in such capacity, here we investigated rats which exhibit, as a trait, opponent attentional biases. These rats are selected from outbred populations using a Pavlovian Conditioned Approach (PCA) test. Goal-trackers (GTs) preferably orient to a Pavlovian reward cue, that is, they learn its predictive significance, but they do not approach and contact such a cue. In contrast, sign-trackers (STs) approach and contact such a cue, which has been interpreted as assigning incentive salience to a Pavlovian cue and attributed to cue-evoked mesolimbic dopamine signaling (Flagel et al., 2011; Flagel and Robinson, 2017; Iglesias et al., 2023). The relatively greater vulnerability of STs for addictive drug taking and relapse in the presence of Pavlovian drug cues has been extensively documented (e.g., Saunders and Robinson, 2010; Yager and Robinson, 2010; Yager and Robinson, 2013).

Goal- and sign-tracking index the presence of broader, opponent cognitive-motivational styles that are dominated by a bias toward deploying top-down (or goal-directed) and bottom-up (or stimulus-driven) processing of action cues, respectively (for review see Sarter and Phillips, 2018; for evidence of the presence of these traits in humans see Schad et al., 2020; Colaizzi et al., 2023). As such biases of GTs and STs were previously shown to be mediated in part via contrasting cholinergic capacities for the detection of cues (Paolone et al., 2013; Koshy Cherian et al., 2017; Pitchers et al., 2017a; Pitchers et al., 2017b), we hypothesized that the cortico-striatal processing of movement cues contributes to the expression of these biases. The present results indicate that cued turning depends on cortico-striatal glutamate signaling in GTs. In contrast, glutamate signaling in STs preferably mediates cued stops and is independent of cortico-striatal neuronal activity.

Materials and Methods

Subjects

378 Sprague Dawley rats (215 females; 250-500 g; obtained from Inotiv, West Lafayette, IN, and Taconic, Rensselaer, NY) were individually housed on a 12-hour light/dark cycle (lights on at 7:00 AM) at ~21ºC with *ad libitum* access to food (Laboratory Rodent Diet 5001, LabDiet) and water. The experiments detailed below used four separate cohorts of rats (each consisted of 52 rats, 26 females and composed of rats obtained from both Taconic and Inotiv). The four cohorts were obtained and formed across 19 months, reflecting the experimental demands of amperometric recordings. All experimental procedures were approved by the University Committee on the Use and Care of Animals (UCUCA) at the University of Michigan and carried out in laboratories accredited by the Association for Assessment and Accreditation of Laboratory Animal Care (AAALAC). Animals acclimated to housing quarters for two days before the onset of experimental procedures.

Behavioral phenotyping

Apparatus. Prior to the onset of PCA testing, rats were handled daily for 3 days and given ~7 banana-flavored sucrose pellets (45 mg; BioServ). Rats were tested in conditioning chambers (20.5 x 24.1 cm floor area, 20.2 cm high; MED Associates Inc.). Each chamber contained a food magazine port located 2.5 cm above the floor in the center of the intelligence panel, a red house light located on the wall opposite the food magazine port (on throughout training sessions), and a retractable lever (Med Associates) located 2.5 cm to the left or right of the food receptacle and 6 cm above the floor. This retractable lever was illuminated when extended with a white LED light placed inside the lever house. For a lever press to be recorded, a force of ~15 g was needed. The pellet dispenser (Med Associates) delivered one 45 mg banana-flavored sucrose pellet (Bio-Serv) into the food magazine port at a time. A head entry was recorded each time a rat broke the infrared photobeam located inside the food magazine port. Each conditioning chamber was placed in a sound-reducing enclosure and a ventilating fan generated background noise. Data collection was controlled by Med-PC IV Behavioral Control Software Suite.

***PCA testing and primary measures*.** One day prior to the onset of PCA testing, rats were placed into the test chamber with the red house light illuminated and the lever retracted. 25 food pellets were delivered in accordance with a variable schedule (VI-30; 0-60 s) to foster the reliable retrieval of pellets from the food magazine port. During PCA testing, trials began by illuminating and extending the lever (CS) for 8 s. Immediately following the retraction of the lever, a single banana

pellet was delivered into the magazine port (US). A variable intertrial interval (ITI; 90±60 s) started immediately after the retraction of the lever. An individual PCA training session consisted of 25 trials and lasted 35-40 min. The following 5 measures were extracted from individual trials and collapsed over individual PCA sessions: (1) number of lever deflections (contacts); (2) latency to first lever deflection; (3) number of head entries into the food magazine port (referred to as food cup entries) during the presentation of the CS; (4) latency to the first magazine port entry after CS presentation; (5) number of magazine port entries during the ITI. Data from animals included in the final analysis reflected sessions during which rats consumed all food pellets.

***Phenotype classification*.** The propensity for rats to approach the lever CS versus the food magazine port during the CS period was expressed by a PCA index score. Briefly, the PCA index score consisted of averaging three measures of the conditioned approach on the 4th and 5th day of testing (e.g., Robinson and Flagel, 2009; Meyer et al., 2012; Yager et al., 2015; Pitchers et al., 2017a; Pitchers et al., 2017b): (1) the probability of contacting either the lever CS or food magazine port during the CS period (P(lever) − P(food port)); (2) the response bias for contacting the lever CS or the food magazine port during the CS period: (# lever CS contacts − # food magazine port contacts)/(# lever CS contacts + # food magazine port contacts); and (3) the latency to contact the lever CS or the food magazine port during the CS period: (food magazine port contact latency − lever CS contact latency)/8. Averaging these three measures yields PCA index scores ranging from −1.0 to +1.0, where +1.0 indicates an animal made a sign-tracking CR on every trial and −1.0 a goal-tracking CR on every trial. Further, rats with an averaged PCA index score ranging from −1.0 to −0.5 were classified as GTs, and rats with a PCA index score between +0.5 and +1.0 as STs.

Cue-triggered turning task (CTTT)

Apparatus. The 32.51 cm wide by 153.67 cm long treadmill was constructed by modifying a 2200 Series Flat Belt End Drive Dorner conveyor (Dorner, WI). The conveyor belt surface material was polypropylene, friction-resistant, and easily cleaned with ethanol or soap. The conveyor was paired with a Dorner Variable Speed Controller (Dorner, WI), with speeds ranging from 0 cm/s to 32 cm/s or 19.2 m/min. The Variable Speed Controller included a reversing controller, allowing the belt to rotate clockwise, "forward," or counterclockwise, "reverse." An in-house-made Faraday cage was placed on top of this conveyer, 145.10 cm long, 32.51 cm wide, and 38.1 cm tall. The wooden frame of the Faraday cage was enclosed by a woven copper mesh and grounded to block out static electric fields. Plexiglass inserts were placed inside the Faraday cage to prevent rodents

from chewing on the mesh. Copper reward ports were installed on either end of the treadmill to allow delivery of 45 mg banana pellets. Experimenters raised two wooden panels on the cage to place rodents on the treadmill. The 28V DC, 100 mA stimulus light was approximately 2.54 cm in diameter with a flat lens and mounted on both sides lengthwise on the Faraday cage (MedAssociates, Inc., St. Albans, VT). The auditory cue was a Mallory-SonAlert audible device. This 28V DC, 18 mA device was mounted on the center of the Faraday cage and was approximately 4.3 cm long by 4.3 cm wide by 3.6 cm tall. This device emitted a continuous tone at 68 dBA sound pressure level, which is within the acceptable range for chronic presentations, to neither elicit a fearful response nor induce hearing loss (Turner et al., 2005; Castelhano-Carlos and Baumans, 2009). These devices were controlled by a MedAssociate interface and a relay module to run our custom program. Performance sessions were videotaped with four web cameras (Logitech C920x HD Pro Webcam, Full HD 1080p/30fps) and relayed to an Intel Xeon workstation (Dell, Round Rock, TX) via USB cords and processed with OBS Studio (Open Broadcaster Software, free and open-source software).

Training regimen. Rats were trained to walk on a treadmill until the onset of one of two cues (tone or sound, presented for 2 s), indicating that following a treadmill stop, 1 s after cue onset, and a 5-s pause, the treadmill restarted in the reverse or same direction, respectively (Avila et al., 2020). Rats learn to respond to turn cues by turning around, and to the stop cue by stopping and not turning. Cued turns and cued stops were rewarded by manually delivering a banana-flavored sucrose pellet (45 mg; Bio-Serv) into the reward port 2-3 s following the treadmill stop.

Rats first underwent a treadmill acclimation regimen using a procedure adapted from Arnold and Salvatore (2014). First, rats were handled for 20 min for two days. On the second day, rats were placed in the Faraday cage for 15 min with the belt paused. All sessions were conducted under dim red lighting to minimize stressors and increase the discriminability of the light cue. For a week, rats were placed into the Faraday cage for 3 min with the belt paused and then trained to walk on the treadmill at speeds up to 9.6 cm/s or approximately 6 m/min. The experimenter manually set the initial rate and direction of the treadmill, with the initial direction counterbalanced within and across subjects. During this training, rats were reoriented by gentle prodding if they began to walk in the opposite direction of the belt. After each session, rats were immediately returned to their home cage and housing room. Between sessions and subjects, the Plexiglass walls of the Faraday cage and the treadmill belt were wiped down with 70% ethanol and soap.

The initial treadmill speed was set at 3.2 cm/s for the first two days and gradually increased by 1.6 cm/s every 2 min. Each session lasted 20 min, so the final walking speed reached 8 cm/s. On the third and fourth days, the initial rate was set at 6.2 cm/s, increasing by 1.6 cm/s every 5 min until the maximum speed of 9.6 cm/s was reached. On the fifth and sixth day, rats walked at 8.0 cm/s for 10 min and 9.6 cm/s for the last 10 min. Finally, on the seventh day of this training regimen, rats walked at 9.6 cm/s for 20 min. In the next training phase, rats were placed on the treadmill and presented with turn and stop cues. The modality of the turn and stop cues was counterbalanced across animals.

Contrary to the acclimation training phase, during which experimenters manually controlled the treadmill, this phase was controlled entirely by custom scripts using Med-PC software and interface (MedAssociates). Rats walked at a speed of 9.6 cm/s and cues were presented for 2 s. Maximally two successive presentations of a cue of the same modality were allowed. The intertrial interval (ITI) was 60±30 s. The total number of trials per daily session was 18, with a maximum duration of a test session of 20 min. Rats underwent cue training for approximately two to three weeks. Then, upon reaching the performance criterion, defined as 70% correct responses to either cue for two consecutive days, rats were tested and videotaped for four additional days. Data from these four sessions were used to determine potential phenotype and sex-based differences in baseline performance. Thereafter, rats underwent surgery for chronic microelectrode array implantation.

CTTT performance measures. Performance measures were cued turns, missed turns, cued stops, and false turns, and extracted from offline scoring of session videos. For a successful turn to be scored, the animal must have initiated a turn, defined by a rotation of the longitudinal orientation of the body of at least 90°, before the treadmill restart, that is, within 8 s of the cue onset. A stop was defined as a cessation of forward movement. For stops occurring before the treadmill stopped, rats would typically stop while positioned at the backend of the treadmill so that following a stop, the treadmill would transport them to the front of the treadmill (within the remaining 1-3 s until the treadmill stopped), without the rat contacting the front end of the test chamber. Following the treadmill stop and during the 5-s pause, a false turn was scored if the animal (falsely) turned. The time of initiation and completion of cued turns, relative to the onset of the cue, were extracted from session videos. For the analysis of baseline CTTT performance, and because rats generated a variable number of cued turns during the 4 sessions used for this analysis, individual turn onset and completion times were averaged across the test sessions. Additional performance measures were extracted from training and testing sessions to explore

relationships between cued turning and stopping performance, phenotype and, subsequently, glutamatergic transients (detailed in Results).

Amperometric recordings of glutamate currents

Electrode preparation and calibration. Extracellular glutamate concentrations were measured by oxidizing glutamate on an electrode surface featuring immobilized glutamate oxidase (GO), and by oxidizing the resulting peroxide levels using fixed-potential amperometry. Based on calibration curves generated *in vitro*, the resulting currents were expressed as micromolar glutamate concentrations at the recording site (Rutherford et al., 2007; Hascup et al., 2008; Parikh et al., 2008; Parikh et al., 2010a; Parikh et al., 2014; Clay and Monbouquette, 2018; Bermingham et al., 2022). The configuration consisted of a ceramic backbone probe (Quanteon LLC, Nicholasville, KY, USA) housing four recording sites, each 15×333 μm, crafted from platinum-iridium (Pt/Ir). These recording sites were grouped into two pairs, separated by 30 μm between each member of a pair and a 100 μm vertical spacing between the pairs, so that the two pairs of electrodes were linearly arranged along the shank of the probe. Microelectrode arrays were modified for *in vivo* recordings in behaving rats by soldering four enamel-coated magnet wires (30 ga) to the terminals on the electrode panel and the other end to gold-pin connectors. Reference electrodes were constructed by soldering Ag/AgCl reference electrodes prepared from 0.008” silver wire (A-M Systems, Carlsberg, WA) to gold-pin connectors. The pins were then inserted into a 9-pin ABS plug (GS09PLG-220, Grinder Scientific) and adhered to the microelectrode with epoxy. Custom 9-pin ABS plugs were also printed with a STUDIO G2 3D printer (BigRep, Berlin, Germany). The top pair of electrodes, termed active sites, were coated with recombinant L-GO (US Biological Life Sciences) solution (1 U in 1 μL DiH2O), cross-linked with a BSA and glutaraldehyde mixture, by manually applying microdroplets using a 1-μl Hamilton syringe. The lower pair of electrodes, termed sentinels, were coated with only the BSA and glutaraldehyde mixture, to record currents unrelated to glutamate concentrations. After a minimum 24-hr incubation period to ensure optimal adherence of the enzyme layer, an exclusion layer composed of *meta*-(1,3)-phenylenediamine (*m*PD) was electroplated onto each recording site's surface by 5-min application of 0.85 V versus an Ag/AgCl reference electrode (Bioanalytical Systems). This exclusion layer prevents sensing electroactive interferents such as ascorbic acid (AA) and catecholamines (e.g., Mitchell, 2004). After another 24-hr incubation period for the electrode sites to dry, recording sites were calibrated to determine the sensitivity for glutamate, selectivity for glutamate versus interferents, stability, and limit of detection of glutamate. Calibrations were conducted using a FAST-16 electrochemical system (Quanteon). A constant voltage of 0.7 V was

applied versus an Ag/AgCl reference electrode, and the system was placed in a heated 40 mL bath of 0.05 M PBS. Following a 30-minute baseline recording, a solution containing 20 mM ascorbic acid (AA, interferent), 20 mM glutamate (analyte), and 2 mM dopamine was introduced to the bath. These additions generated the following concentrations: 250 μM AA, 20, 40, and 80 μM glutamate, and 2 μM dopamine. Changes in amperometric current at individual electrode sites were measured after each solution to calculate the slope (sensitivity), the limit of detection, selectivity for AA and dopamine, and linearity (R^2). Glutamate sensors were required, at a minimum, to have a sensitivity of >5 pA/μM glutamate, a limit of detection <1.0 μM glutamate, glutamate:AA selectivity ratio >50:1, and a linear response to increasing glutamate concentrations (20-80 μM glutamate) of R >0.95. The characteristics of the electrodes used in the present experiments exceeded these minimum requirements (Table 1).

Insert Table 1 about here

Chronic implantation of microelectrode arrays (MEAs). Upon having reached stable, criterion-level performance CTTT (≥70% cued turns and stops for two consecutive days), microelectrode arrays were chronically implanted into the DMS. Rats were anesthetized using isoflurane gas (5% induction and 1–3% maintenance) and mounted on a stereotaxic frame on a heating pad to maintain a 37°C body temperature. Ophthalmic ointment lubricated eyes. A craniotomy and durotomy using a bent 27-gauge needle for dura removal were performed above the right DMS (AP: +0.50 mm; ML: −2.20 mm from bregma). Three stainless steel screws were threaded into the cranium. The MEA was then lowered 4.5 mm dorsoventrally from the dura into the striatum. At the same time, an Ag/AgCl reference electrode was implanted at a remote site in the contralateral hemisphere. The microelectrode assembly was anchored with methyl methacrylate dental cement, and exposed regions of the skull were filled with a translucent, medium-viscosity silicone adhesive to minimize leakage of the dental cement onto the brain. Animals rested over a 48-hour recovery period before moving to the next phase of the experiment. Amperometric recordings were collected by connecting the head stages to a FAST-16 potentiostat/data electrochemical system (Quanteon) via a shielded cable and low-impedance commutator. The hydrogen peroxide by-product of GO catalyzation was electrochemically oxidized by applying 0.7 V versus the Ag/AgCl reference electrode and digitized at a sampling rate of 5 Hz. Behavioral sessions began following a 50-minute baseline recording period. Consistent with prior evidence

showing that implanted MEAs maintain stable sensitivity and reliability for at least seven days after implantation, electrochemical recordings were completed within seven days of MEA implantation (Rutherford et al., 2007).

Amperometry data processing and analysis of glutamate peaks. Electrochemical recording data were processed using a custom MATLAB (MathWorks) script. The background current recorded on sentinel sites was subtracted from the current recorded on the active sites, normalized by the response to dopamine, and then converted to glutamate concentration based on calibration curves. Trial-associated glutamate concentrations were determined over 13-s bins, involving the following task-related periods: 3 s prior to the onset of turn and stop cue presentation, throughout cue presentation (2 s), and until the treadmill stopped (1 s after cue offset), during the subsequent 5 s pause when the reward was delivered and retrieved, and for 2 s following the restart of the treadmill belt. The concentration of glutamate currents recorded over 2.5 s prior to cue onset (approximately 10 data points), served as a baseline for analyzing glutamate levels for each trial. Changes from these baselines were used for statistical analyses (e.g., Parikh et al., 2007a) and, therefore, glutamate concentrations shown in graphs depict sentinel-corrected, normalized and baseline-corrected levels. Although minimal drift of baseline glutamate levels was seen across trials and sessions, such baseline-based correction reduced the impact of potential minute-based variations in glutamate concentrations.

The analysis of glutamate concentrations focused on the maximum peak concentrations and, secondarily, the timing of the first peak relative to cue onset and reward delivery, and the number of peaks within 1.5 s of these events. Prior studies on the effects of depolarization of synaptic terminals, blocking such depolarization, or of pharmacological manipulations of the excitability of terminals, confirmed that peak concentrations of extracellular glutamate indicate the extent of terminal depolarization (Hascup et al., 2008; Parikh et al., 2008; Parikh et al., 2010b; Mattinson et al., 2011; Quintero et al., 2011; Parikh et al., 2014). The PeakDet function in MATLAB (MathWorks) was utilized to identify peaks, requiring setting threshold and minimum differences. To be identified as a peak, glutamate concentrations needed to be 3 standard deviations (SD) above the average baseline current (recorded over 2.5 s before cue presentation). In addition, for a value to be identified as a peak, the preceding and subsequent values needed to be at least 1 SD (derived from baseline data) below the peak value. These parameters were adopted from peak analyses in neurophysiological studies (e.g., Ghosh et al., 2022) and ensured a robust separation of peaks from potentially noisy recordings of relatively small currents.

For each response category (cued turns, misses, cued stops, false turns), glutamate traces were included into the final analyses if; a) if the electrode met the *in vitro* calibration criteria, b) traces were devoid of major electrostatic interferences (such as resulting from the headstage contacting the reward port); c) task compliance was apparent (animals walking continuously counter the direction of the treadmill and promptly reversing direction upon cue or treadmill onset)**;** d) the accuracy of the electrode placement was confirmed, determined following the completion of experiments. The data from a rat that developed seizures after the 2nd day of recordings were completely excluded from the final analyses. As a result, 1-27 (range) traces per rats and response categories were included in the final analyses.

The maximum peak concentration (µM), time to peak (s), and number of peaks were extracted from each trace used for the final analyses. Peak amplitude was defined as the highest glutamate concentration reached within 1 s from the onset of a cue or from reward delivery. The time to peak was defined as the time from cue onset or reward delivery to the first peak. During missed turns, peaks were not identified in a small fraction of trials (<2% in both phenotypes), yielding missed data for this measure. The number of peaks were counted across a 1.5-s period from cue onset or reward delivery.

Verification of MEA placements in the DMS. Microelectrode arrays (MEAs) were chronically implanted into the DMS to record extracellular glutamate levels while performing the CTTT. Following the completion of experiments, administration of a lethal dose of sodium pentobarbital (270 mg/kg, i.p.) was followed by transcardial perfusion of saline, followed by 4% paraformaldehyde in 0.15 m sodium-phosphate solution, pH 7.4. Extracted brains were postfixed in 4% paraformaldehyde for 24 hrs, then submerged in 30% sucrose solution until they sank. Using a freezing microtome (CM 2000R; Leica), 35-µm thick brain slices were sectioned and stored in cryoprotectant until further histologic processing. Sections were mounted and processed with a Cresyl Violet Nissl stain to confirm MEAs placement. A Leica DM400B digital microscope was used to photomicrograph the sections at 1.25X and 5X magnification at three A-P levels (0.2 mm, 0.5 mm, and 1.0 mm).

Intracranial infusions of a Cre-dependent DREADD and a retrograde Cre-vector

We utilized a pathway-specific dual-vector chemogenetic strategy (e.g., Sherafat et al., 2020) to selectively inhibit the activity of fronto-cortical projections to the DMS. Intracranial infusions of a Cre-dependent Designer Receptor Activated Only by Designer Drug (DREADD) and a retrograde were carried out following PCA screening and prior to CTTT acquisition training. In a subset of

rats, a second surgery, carried out following the acquisition of the CTTT, was conducted to implant electrochemical recording electrodes into the DMS. The viral vectors containing the Cre-dependent plasmid pAAV-hSyn-DIO-hM4D(Gi)-mCherry (AddGene #44362-AAV8; titer of 2.1x1013 GC/mL), Cre-dependent control plasmid pAAV-hSyn-DIO-mCherry (AddGene #50459-AAV8; titer of 2.2x1013 GC/mL), or the retrogradely transported Cre-expressing plasmid pENN-rAAV-hSyn-HI-eGFP-Cre-WPRE-SV40 #105540-AAVrg; titer of 1.9x1013 GC/mL) were infused into the lower layers of the prelimbic cortex (for the anatomical organization of fronto-striatal projections see, e.g., Mailly et al., 2013) and the DMS, respectively.

Craniotomies and durotomies were carefully performed above four sites of the DMS using a bent 27-gauge needle for dura removal to minimize the impact on the subsequent implantation of recording electrodes and electrochemical recordings. One µL of pENN-rAAV-hSyn-HI-eGFP-Cre-WPRE-SV40 vector was infused (bolus) into the DMS at two sites per hemisphere (AP: +0.2/1.2; ML: ±2.5/2.2; DV: -4.5 mm from dura) to retrogradely transfect afferent projections. In addition, one µL of AAV-hSyn-DIO-hM4D(Gi)-mCherry or AAV-hSyn-DIO-mCherry (control vector) was infused (bolus) into the prelimbic cortex (AP: +3.2; ML: ±0.7; DV: -3.5 mm from dura) to allow for the selective inhibition of cortico-striatal projections. The injector was left in place for 8 min to minimize diffusion into the injector tract. Rodents recovered for one week before treadmill and CTTT training.

Clozapine N-oxide (CNO). CNO was obtained from Tocris Bioscience (Bristol, United Kingdom) and dissolved 10 mg/ml in 6% DMSO in 0.9% NaCl solution. CNO (5.0 mg/ml/kg; i.p.) or vehicle was administered i.p. 50 min before the onset of CTTT testing. In rats also equipped for electrochemical recording of dorsomedial GLU levels, CNO was given just prior to the onset of the pre-task GLU baseline (above). Rats were given vehicle and CNO on alternate days. Regarding potential off-target effects of clozapine (Gomez et al., 2017), we and others have previously consistently failed to detect effects of this dose of CNO in rats expressing the control vector, including in rats performing the CTTT, complex movement control tasks, or an operant sustained attention task (Jendryka et al., 2019; Avila et al., 2020; Kucinski et al., 2022). Given effective dose ranges of clozapine in rodents performing complex behavioral tasks (Martinez and Sarter, 2008), and given the proposed conversion rate of CNO to clozapine, an approximately 50-100-fold higher dose of clozapine would be required to produce significant effects (see also Mahler and Aston-Jones, 2018; Lawson et al., 2023).

Visualization and quantification of GFP/mCherry-expressing neurons. We amplified the mCherry fluorescent reporter signal of the inhibitory hM4Di DREADD vector to enhance the evaluation of the transfection efficacy and distribution of neurons expressing mCherry and eGFP, the latter indicating the expression of the retrograde Cre-expressing vector in frontal cortex. The eGFP fluorescent label did not necessitate signal enhancement. Sections underwent six washes for 5 min each in 0.1 m PBS, pH 7.3, and then were immersed in 0.1% Triton X-100 diluted in PBS for 15 min. After three 5-min PBS rinses, sections incubated for 60 min at room temperature (RT) in the blocking solution, 1% normal donkey serum (NDS) and 1% Triton X-100 made in PBS. Sections were incubated overnight in the primary antibody (rabbit anti-mCherry, ab167453, Abcam; 1:500; diluted in blocking solution to prevent non-specific binding). The next day, and following three 5-min PBS rinses, sections were incubated for 90 min at RT in the secondary antibody (donkey anti-rabbit conjugated to Alexa 594, PIA32754, Invitrogen, 1:500). Following three 5 min-rinses with PBS and sections were mounted, air dried, and cover-slipped with Vectashield Antifade Mounting Medium (H-1000; Vector Laboratories).

A Zeiss LM 700 confocal microscope, equipped for sequential multi-track acquisition with 488- and 561nm excitation lines, along with specific filter sets for Alexa 488 (Zeiss filter set 38 HE) and Alexa 594 (Zeiss filter set 54 HE), was employed for visualizing and capturing images of fluorescent neurons. Images were taken at magnifications of 10x to confirm placements of infusions in the DMS, 20x and 40x at five anterior-posterior levels (frontal cortex: 3.0 mm and 3.24 mm, striatum: 1.2 mm, 0.5 mm, and 0.2 mm) for verification and documentation of single and double-labeled cells in cortex and striatum.

We employed a modification of a prior, semi-quantitative estimation of transfection efficacy and space (Avila et al., 2020). Briefly, GFP labeling that was centered in the striatal target region of prelimbic projections (Mailly et al., 2013) was assigned the highest transfection score (5), whereas labeling that extended into more lateral and ventral regions and only partially covered the target region were assigned lower scores. Likewise, mCherry labeling that exclusively covered the entire prelimbic cortex was assigned the highest score. Partial expression of mCherry in this region, or labeling that extended dorsally or ventrally beyond the prelimbic cortex, were assigned lower transfection efficacy scores. Furthermore, single-and double-labeled neurons were counted in the prelimbic region, and the proportion of double-labeled neurons was computed for each rat. Counting frames were superimposed on each subregion using the ImageJ multipoint tool. Cells were counted on two sections per brain, yielding four counts per brain and subregion. Averaged counts obtained from each brain and subregion were used for further analyses. To produce

images of neurons expressing mCherry and GFP, and control for potential “bleed-through” (e.g., North, 2006),we used the split view feature within Zen Black software (ZEN 2.31 SP1 Black Edition; Zeiss) for examination of individual channels with multi-track images. Tile scanning/stitching techniques were implemented at both 10x (3 × 2 tiles, covering an area of 3455.94 by 2370.64 μm) and 20x magnifications (4 × 3 tiles, covering an area of 1407.88 by 1135.31 μm).

Experimental design and statistical analyses

Behavioral data. Chi-square tests were used to determine the effects of sex and the commercial source of rats (vendor) on the distribution of PCA screening scores. Baseline CTTT performance was analyzed using conventional repeated measures ANOVAs; associated graphs depict individual values, means, and 95% Confidence Intervals (CI). Conventional ANOVAs were computed using SPSS for Windows (version 28.0; SPSS) and GraphPad Prism (version 10.1.2).

Glutamate concentrations and effects of CNO. Extracellular glutamate concentrations were sentinel-corrected, normalized to dopamine, and pre-cue baseline corrected (see above for details). From these data, peak concentrations and peak timing information were extracted (see above for the definition of the three measures and of peaks). Given the complexity of the experimental design (variable number of rats per phenotype, turn and stop trials, and of cue-evoked glutamatergic transients), here we first determined potential phenotype-specific differences in glutamate peaks across trial types and response categories, followed, in cases, by *post hoc* analyses of event-related glutamate levels within individual phenotypes. Linear-mixed effects models (LMMs) with restricted maximum likelihood estimation were employed by SPSS for Windows (version 28.0; SPSS). A key reason for using LMMs concerned the definition of sample size (number of animals versus the number of individual traces collected from each animal). Moreover, sample sizes may vary across repeated or otherwise dependent measures (e.g., Schielzeth et al., 2020; Yu et al., 2022). Data from repeated sessions were used to compute the repeated fixed effect, and phenotype was used to determine between-subjects fixed effects, with a subject identifier random intercept. Separate LMMs were computed for the analysis of glutamate levels during four response categories (cued turns, missed turns, cued stops, reward delivery); the three measures analyzed per response categories (maximum peak levels, time to first peak, and number of peaks; defined above) were treated as dependent measures. The covariance structures with the lowest Akaike’s information criterion were selected for each model (Verbeke and Molenberghs, 2009). Main effects of phenotype derived from the analysis of the

three measures were followed up using Bonferroni's method for pairwise comparison of the means. When LMMs reported significant interactions, repeated measures ANOVAs were used to compare data from repeated sessions, with Huynh–Feldt-corrected *F* values and corrected degrees of freedom applied in case of violation of the sphericity assumption. Data graphs showing glutamate concentrations depict individual values, estimated marginal means (EMMs), and 95% CI.

Contingency table analyses. Glutamate trace characteristics were extracted from 548 recordings of turn cue trials, 364 of which yielded a turn (GTs: 206, STs: 158) and 184 a miss (GTs: 112, STs: 72). Contingent on threshold maximum peak concentrations, and the presence of a single or multiple cue-evoked glutamate peaks, the proportions of turns and misses were compared using contingency table analyses (*P* values were computed using Fisher's exact test; GraphPad Prism). Furthermore, the relative probability for turns in GTs, as well as the reciprocal value, were derived from these analyses (Koopman asymptotic score; Koopman, 1984; Motulsky, 2018).

Effects of CNO on CTTT performance. The effects of CNO or its vehicle on cued turns and stops, in rats expressing the inhibitory DREADD or the empty control vector, were analyzed using repeated measures ANOVA (general linear model) on the effects of phenotype and treatment day. For clarity, effects on the two behavioral measures were analyzed separately, at alpha=0.05/2. Tukey's Honest Significant Difference test was used to compare, *post hoc*, the effects of the 1st and 2nd administration of CNO with the effects of the 1st and 2nd administration of vehicle (GraphPad Prism).

P values and effect sizes. Exact *P* values were reported (Greenwald et al., 1996; Sarter and Fritschy, 2008; Michel et al., 2020). For key findings, effect sizes were computed using generalized eta squared (η_p^2) (effect sizes of 0.02 typically are classified as small, 0.13 as medium, and 0.26 as large; e.g., Bakeman, 2005), derived from Bonferroni pairwise comparisons of estimated marginal means (Greenwald et al., 1996).

Results

Phenotype screening and distribution by sex and vendor

PCA screening generated five behavioral measures indicating the speed and frequency of contacting the lever (Pavlovian CS) versus the speed and frequency of head entries into the food port. These measures were collapsed into the PCA score, indicating the degree of sign-tracking and goal-tracking, respectively, of individual rats over 5 PCA test sessions. Prior analyses have consistently shown that all rats orient toward the CS, that is, all rats learn the predictive significance of the CS, but only some – the STs – approach and contact the CS (Fig. 1a, top right photo), while GTs do not contact the CS but approach and enter the food port (Fig., 1a, bottom right photo; e.g., Robinson and Flagel, 2009; Meyer et al., 2012; Pitchers et al., 2017a).

Insert Figure 1 about here

PCA scores from the last two sessions were averaged and used to classify rats as STs and GTs. PCA screening of N=378 (215 females) rats yielded 113 GTs (30%), 155 rats with intermediate scores (INs; 41%; not shown), and 110 STs (29%). Figure 1a shows the distribution of PCA scores across the five test sessions of the rats used for CTTT training and amperometric recordings (79 rats GTs, 13 females; 22 STs, 13 females; data from rats with intermediate PCA scores are not shown).

As PCA screening was conducted in four separate cohorts of rats, separated by 2-19 months, we first determined that PCA scores did not differ across these cohorts (no main effects of cohort on response bias (respbias), probability difference (probdiff), latency, or PCA index; all F<1.74, all P>0.16). Chi-square tests were used to determine if sex or the commercial source of the rats (vendor) influenced the distribution of phenotypes. Consistent with prior reports (Pitchers et al., 2015), the distribution of PCA scores did not differ by sex ($X^2(2, N=378)$=01.63, P=0.44; Fig. 1b). However, the distribution of PCA scores from rats obtained from the two vendors differed significantly ($X^2(2, N=378)$=36.62, P<0.001; Fig. 1c). Relatively more rats obtained from Inotiv displayed lever-directed behaviors, while rats supplied by Taconic relatively more frequently exhibited goal cup-directed behaviors. A follow-up analysis rejected the possibility that vendor-specific PCA score distribution differed by sex (Inotiv: $X^2(2, N=133)$=1.30, P=0.52; Taconic: $X^2(2,$

N=245)=1.41, *P*=0.50. GTs and STs of both sexes and from either vendor were combined for use in subsequent experiments.

Cue-triggered turning task (CTTT) acquisition and criterion performance

Upon reaching criterion performance in the CTTT (see task illustration in Fig. 2a-c), defined as >70% cued turns and cued stops for two consecutive days/sessions, and prior to the intracranial implantation of microelectrode arrays, the relative number of cued turns and stops were recorded from an additional 4 test sessions to determine baseline CTTT performance of GTs and STs.

Insert Figures 2 and 3 about here

The number of training sessions required by GTs (n=29, 13 females) and STs (n=22, 12 females) to reach CTTT criterion performance, defined as 70% correct responses to either cue for two consecutive sessions, did not differ significantly ($F(1,47)=0.01$, $P=0.94$; Fig. 3a). Likewise, males and female rats acquired this task at comparable rates (main effect of sex: $F(1,47)=0.81$, $P=0.37$; phenotype x sex: $F(1,47)= 0.27$, $P=0.61$).

After having reached performance criterion, GTs scored significantly more cued turns than STs across four subsequent test sessions (main effect of phenotype: $F(1,47)=5.03$, $P=0.003$, $\eta_p^2=0.097$; GTs: 0.80 (mean) cued turns/trials; STs: 0.73; note that while Figs. 3b and c show response ratios, ANOVAs were conducted with arcsine-transformed values because ratio data violated homoscedasticity). A main effect of day (or session; $F(3,141)= 4.96$, $P=0.003$, $\eta_p^2=0.096$) reflected that rats generated more cued turns during the third when compared with the first of the four sessions used for the determination of CTTT baseline performance (Fig. 3b; day 1: 0.71 (mean) cued turns/trials; day 3: 0.83). Sex did not affect turning rates ($F(1,47)=0.01$, $P=0.95$) and interactions between phenotype, sex and day remained insignificant (all $F<2.10$, all $P>0.15$). Cued stops did not differ by phenotype, day or sex (all main effects and interactions: all $F<3.06$; all $P>0.052$; Fig. 3c).

Relative to the time of cue onset, GTs initiated and completed cued turns significantly later than STs (main effects of phenotype; initiation: $F(1,51)= 8.84$, $P=0.005$, $\eta_p^2=0.16$; completion: $F(1,51)= 9.40$, $p=0.004$, $\eta_p^2=0.17$; Fig. 3d; effects of sex and interactions between the effects of sex and phenotype: all $F<1.03$, all $P>0.32$). Reflecting the parallel effects of phenotype on initiation and

completion time, the time needed to complete turns did not differ between the phenotypes (main effects of phenotype, sex, and interactions: all $F<3.51$, all $P>0.07$); GTs: 2.69±0.15 s (M, SEM); STs: 2.33±0.17 s; not shown).

Taken together, GTs and STs acquired the CTTT within a similar number of training sessions, GTs scored more cued turns than STs, and GTs initiated and completed cued turns at significantly later times relative to cue onset. Subsequent experiments recorded mediodorsal striatal glutamatergic transients during cued turns and stops, missed turns and false turns, and tested the role of fronto-striatal glutamatergic projections in generating performance-associated glutamatergic transients. Because of the absence of significant effects of sex and interactions involving sex in the analysis of baseline CTTT performance, subsequent statistical analyses, using linear mixed effect models to account for effects of animals and variable numbers of transients recorded from each animal, did not further involve sex as a statistical variable. Furthermore, cue modality did not impact turn or stop rates and thus, likewise, was not included as a factor in the final analyses.

Turn and stop cue-locked, phenotype-specific dorsomedial glutamate dynamics

Rats were screened for the classification of the phenotypes, underwent CTTT training until they performed at criterion level, followed by implantation of an MEA into the DMS and subsequent recordings of glutamate currents during CTTT performance. Figure 4 illustrates the four recording sites fabricated onto a ceramic backbone (Fig. 4a) and the preparation of pairs of recording sites for the measurement of glutamate concentrations and potential electroactive interferents (Figs 4b,c). Following calibration of the electrodes *in vitro* (Table 1; a representative example is shown in Fig. 4d), MEAs were permanently implanted into the DMS (Fig. 4e). Examples of currents, recorded via GO-sensitive electrodes (Fig. 4f) and sentinels (Fig. 4g), serve to illustrate the resulting, subtracted current (Fig. 4h). Using sentinel- and pre-cue baseline-corrected traces, glutamate concentration peaks (Fig. 4i) were identified using a MATLAB tool (data points that were >3 SD above baseline levels and >1 SD above adjacent data points (see Methods). Peaks of extracellular glutamate at the active electrode surface may reflect the orchestrated yet asynchronous depolarization of glutamatergic terminals, over several hundreds of milliseconds and within fractions of micrometers from the electrode surface, and likely sufficient to stimulate synaptic and extra-synaptic, relatively low-affinity GLU receptors (Hascup et al., 2008; Parikh et al., 2008; Parikh et al., 2010b; Mattinson et al., 2011; Quintero et al., 2011; Parikh et al., 2014),

(e.g., Clements et al., 1992; Rusakov and Kullmann, 1998; Budisantoso et al., 2013; Matthews et al., 2022; Mendonca et al., 2022).

Insert Figure 4 about here

Figure 5a shows representative glutamate currents obtained from a GT and a ST during a cued turn (peaks are symbolized as circles; horizontal bars indicate the timing of the actual turn). The recording from the GT indicated a peak for the first data point after cue onset, followed by a maximum peak. In contrast, in the ST, only the third data point after cue onset was the first peak, and also the maximum peak, locked to the turn cue, and it was followed by 2 more peaks within 1 s following that first peak. The maximum, turn cue-locked peak concentration was higher in the GT than the ST. Reward delivery elicited two additional peaks in the ST, but none in the GT.

Insert Figure 5 about here

LMMs were used to analyze phenotype-dependent maximum peak glutamate concentrations within 1 s of the onset of turn and stop cues and of reward delivery, time to first peak, and the number of peaks occurring within 1.5 s of cue onset or reward delivery. Maximum glutamate peak concentrations recorded during cued turns were significantly higher in GTs than in STs (phenotype: $F(1,28.85)= 8.85$, $P=0.006$, $\eta_p^2=0.23$; Fig. 5b). In contrast, maximum peak amplitudes locked to other task events all were significantly higher in STs (missed turns: $F(1,193)= 55.20$, $P<0.001$, $\eta_p^2=0.22$, Fig. 5c; cued stops: $F(1,27.67)= 33.32$, $P<0.001$, $\eta_p^2= 0.55$, Fig. 5d; reward delivery (during cued turn trial): $F(1,19.28)= 28.88$, $P<0.001$, $\eta_p^2= 0.40$, Fig. 5e; errors in response to stop cues were extremely rare and thus not analyzed). In addition, in GTs, turn cue-locked increases in glutamate concentrations rose faster (time to first peak: phenotype: $F(1,19.38)= 7.10$, $P=0.02$, $\eta_p^2=0.27$, GTs: 0.69 s; STs: 0.76 s) and peaked less frequently (number of peaks: $F(1,27.81)= 13.80$, $P<0.001$, $\eta_p^2=0.33$, GTs: 1.28 peaks; STs: 1.59) than in STs (not shown). Significant phenotype-specific effects on time-to-peak and the number

of peaks locked to other task events were less consistent (missed turns: faster peak times in GTs ($F(1,193)=5.43$, $P=0.02$) but similar peak numbers; cued stops: similar peak times but more peaks in GTs ($F(1,29.21)= 18.24$, $P<0.001$); reward delivery: similar peak times and numbers; not shown).

Glutamate trace characteristics predicting cued turns

Glutamate trace characteristics were extracted from 548 recordings of turn cue trials, 364 of which yielded a turn (GTs: 206, STs: 158) and 184 a miss (GTs: 112, STs: 72), to determine whether such characteristics, individually or in combination, disproportionally predicted more cued-triggered turns in GTs or STs. Contingency tables were used to compare phenotype and outcome-specific proportions and to compute the probability for turns in GTs relative to STs.

Insert Figure 6 about here

Turn cue-evoked glutamate peak concentrations greater than 2.8 µM were followed by disproportionally more turns in GTs than STs (2.8-8 µM: $P=0.045$-<0.0001). With increasing glutamate maximum threshold concentrations, GTs were 1.12 (>2.8 µM) to 1.40 (>8 µM) times as likely as STs to turn (Fig. 6; concentrations >10 µM yielded contingency table cell counts of n<10 and thus were not included).

Furthermore, if one single glutamate peak occurred following the onset of turn cues, GTs were 1.43 times as likely as STs to turn ($P<0.0001$). In addition, if only one single glutamate peak followed the turn cue, increasing amplitudes of these peaks predicted significantly higher relative probabilities for turns in GTs, plateauing at >4 µM where GTs were 1.73 times as likely as STs to turn (Fig. 6, top curve; note that all data points of this curve reflect highly significant phenotype-dependent differences in the proportion of turns and misses).

In contrast to the significantly higher odds for turns in GTs following a single cue-evoked glutamate peak, following 2 and 3 glutamate peaks (no more than 3 peaks were observed), GTs were only 0.74 times as likely as GTs to turn (or STs were 1.35 times as likely as GTs to turn; $P<0.0001$). However, in the presence of 2 or 3 glutamate peaks, increasing maximum peak levels again increased the probabilities of GTs to turn, so that at maximum peak threshold levels >4 µM, GTs

were as likely as STs to turn (both $P>0.85$; Fig. 6, bottom curve).

Irrespective of whether a single or multiple glutamate peaks were evoked by the turn cue, increasing maximum glutamate concentrations increased the relative probabilities of GTs to turn. This observation was substantiated by the finding that the slopes of the linear regressions of both curves (top and lower in Fig. 6) were different from zero (both $P<0.0001$). However, the absolute differences between single- versus multi-peak-contingent probabilities are noteworthy. Comparing the relative turn probabilities at maximum peak concentrations >4 µM, GTs were 1.002 times *more* likely (or nearly exactly twice *as* likely) as STs to turn if the number of cue-evoked glutamate peaks was limited to one.

Together, these analyses of glutamate trace characteristics indicated that, individually, increasing maximum peak glutamate concentrations and the presence of a single, cue-evoked glutamate peak strongly increased the relative probability of GTs to execute a cued turn. Moreover, the combination of these two properties yielded significantly even higher relative turn probabilities in GTs (Fig. 6). In contrast, the presence of multiple glutamate peaks, GTs were significantly less likely than STs to turn although, when combined with high (<4 µM) maximum peak concentrations, turn proportions of the two phenotypes no longer differed significantly. These findings suggest fundamentally different turn cue-evoked glutamate release dynamics in GTs versus STs, perhaps involving separate afferent circuitry influencing the excitability of cortico-striatal glutamatergic terminals. Therefore, we predicted that inhibition of the cortico-striatal neurons affects turning rates and cued turn-evoked glutamate peaks primarily in GTs, consistent with prior evidence indicating their relative reliance on top-down, cortico-fugal systems to execute cued responses.

Inhibition of fronto-striatal projection disrupts cued turning and turn cue-evoked GLU in GTs, but not STs

As described above, in GTs, cued turning was mediated via tightly orchestrated single glutamate release events that were closely locked to the turn cue, comparable with cue-evoked cholinergic transients in cortex (Parikh et al., 2007b; Gritton et al., 2016; Howe et al., 2017) and therefore hypothesized to reflect cortico-striatal activation. In contrast, in STs, more slowly rising, multiple glutamate release events, as well as the presence of relatively larger reward delivery-locked glutamate release, may have reflected the impact of intra-striatal circuitry and ascending, including dopaminergic, inputs on the excitability of glutamatergic terminals of cortico-striatal projections (e.g., Tritsch and Sabatini, 2012; Agnoli et al., 2013; Dautan et al., 2020; Moss et al., 2021). We tested the hypothesis that turn cue-locked glutamate peaks in GTs reflect cortico-

striatal activation by using a dual vector approach to express an inhibitory DREADD in fronto-striatal projection neurons.

Insert Figure 7 about here

Following PCA screening, GTs (n=12, 6 females) and STs (n=10, 4 females) underwent surgery to infuse an inhibitory DREADD vector into the prelimbic cortex and a Cre-expressing, retrogradely transported plasmid into the DMS (see Fig. 7 for a timeline and a schematic illustration of the dual vector strategy used to inhibit cortico-striatal projections). An additional group of GTs (n=5, 2 females) and STs (n=2, 2 females) received infusions of a mCherry expressing control vector into the prelimbic cortex, in addition to the Cre-expressing plasmid into the striatum, to allow for the assessment of potential off-target effects of CNO. Following this surgery, all rats were trained to CTTT performance criterion. Thereafter, the effects of CNO or vehicle on CTTT performance were assessed in n=14 rats (9 GTs, 3 females, 5 STs, 4 females; Fig. 7c). The remainder of the rats (8 GTs, 4 females, 7 STs, 2 females) underwent a second surgery to implant glutamate recording electrodes into the DMS (Fig. 7d), followed by the assessment of the effects of CNO on performance and glutamate transients (Fig. 7d).

CNO disrupts cued turns in GTs. On the first of 4 days of testing of the effects of CNO or vehicle, and when the vehicle for CNO was administered, the number of turns/turn cue trials and the number of stops/stop cue trials did not differ significantly between animals without (Fig. 7c) and with (Fig. 7d) implanted MEAs (both $t<0.65$, both $P>0.53$, at alpha=0.05/2). Thus, for the initial analysis of the effects of CNO on CTTT performance, data from both subgroups were collapsed. The effects of CNO/vehicle in GTs and STs on cued turns and cued stops were analyzed individually, using ANOVA of the effects of phenotype and day (repeated measures ANOVA, with alpha=0.05/2).

In rats expressing the inhibitory DREADD, administration of CNO reduced the relative number of cued turns in GTs but not STs (main effect of phenotype: $F(1,20)=9.45$, $P=0.006$; main effect of day: $F(3,60)=17.27$, $P<0.0001$; phenotype x day: $F(3,60)=16.30$, $P<0.0001$; see Fig. 7e for multiple comparisons). As reflected by the size of the effect of CNO in GTs ($\eta_p^2=0.72$), the number of cued turns in GTs were approximately halved by the administrated of CNO. In contrast, CNO

did not affect the relative number of cued stops (main effect of day: F(3,60)=0.18, *P*=0.89; day x treatment: F(3, 60)=0.26, *P*=0.86; main effect of phenotype: F(1,20)=5.14, *P*=0.04, n.s. at alpha=0.05/2, reflecting a trend for relatively more cued stops in GTs; Fig. 7f). In rats expressing the empty control vector, CNO affected neither the relative number of cued turns (all F<2.14, all *P*>0.17) nor cued stops ((all F<1.13, all *P*>0.43; not shown).

CNO attenuates turn cue-locked glutamate peaks in GTs. Guided by the results illustrated in Figs. 5 and 6 and using identical peak definitions and extraction methods, the analyses of the effects of CNO on glutamate transients focused on cue-evoked maximum peak concentrations and the number of peaks. Linear mixed-effects models were used to analyze the effects of CNO or vehicle on glutamate transients recorded from GTs and STs expressing the inhibitory hM4Di DREADD or the empty control construct. Glutamate peaks from cued turns, missed turns, cued stops, and false turns were analyzed (Fig. 7g-j).

Administration of CNO significantly reduced turn cue-locked maximum peak glutamate concentrations in GTs, but not STs (phenotype x treatment: (*F*(1,200.79)=18.42, *P*<0.001; main effect of treatment: *F*(1,200.79)=44.76, *P*<0.001; phenotype: *F*(1,9.50)=0.73*, P*=0.41, reflecting the efficacy of CNO in GTs, yielding statistically similar glutamate concentrations in both phenotypes: GTs: 8.61±0.69 µM, STs: 7.77±0.70 µM). Multiple comparisons (shown in Fig. 7g) indicated that CNO significantly suppressed turn cue-locked maximum peaks in GTs (η_p^2=0.21), but not STs, and that following the administration of vehicle, GTs again (see Fig. 5b) exhibited higher maximum peak levels than STs. CNO reduced maximum peaks in GTs to statistically similar levels seen in STs irrespective of treatment (Fig. 7g).

As seen before, the number of glutamate peaks seen during cued turns was significantly higher in STs than in GTs (main effect of phenotype: *F*(1,11.72)=8.10, *P*=0.02; GTs: 1.74±0.15 peaks (M, SEM); STs: 2.38±0.17). CNO administration increased the number of peaks only in GTs, as was indicated by a significant interaction between the effects of treatment and phenotype and multiple comparisons (F(1,73)=3.83, *P*=0.04, η_p^2=0.05; GTs/SAL:1.51±0.16 peaks; GTs/CNO: 1.96±0.18; STs/SAL: 2.32±0.18; GTs/CNO: 2.44±0.19; not shown).

Residual turns following CNO in GTs. CNO robustly reduced cued turn rates in GTs (Fig. 7e). Furthermore, we observed CNO-attenuated maximum glutamate peaks (Fig. 7g) during (residual) cued turns, raising the question whether these residual turns differed behaviorally from those seen in vehicle-treated GTs. Thus, we compared residual cued turns following CNO with turns executed following vehicle administration and, guided by the turn initiation time data shown in Fig.

3d (baseline performance), focused on this parameter. Based on data from individual trials (Fig. 7h), administration of CNO significantly increased the time GTs took to initiate turns when compared with STs (LMM; phenotype x treatment: $F(1,173.72)=9.70$, $P=0.002$, $\eta_p^2=0.05$; see Fig. 7h for multiple comparisons). As before (Fig. 3d), GTs took more time to initiate the turn (main effects of phenotype: $F(1,14.02)=9.69$, $P=0.01$, $\eta_p^2=0.41$; treatment: $F(1,173.72)=30.34$, $P<0.001$, $\eta_p^2=0.15$).

To gain further insight into the effects of CNO, a second analysis of this data was based on the average turn initiation times of individual rats following the two treatments (Fig. 7i). Main effects of phenotype ($F(1,13)=7.34$, $P=0.02$, $\eta_p^2=0.36$) and treatment ($F(1,13)=39.82$, $P<0.001$, $\eta_p^2=0.75$) reflected that GTs generally took more time to initiate turns than STs, and that CNO generally increased the time from cue onset to the initiation of turns. Furthermore, following the administration of CNO, turn initiation times became significantly slower in GTs relative to STs, as was supported by a significant interaction between the two factors ($F(1,13)=7.15$, $p=0.02$, $\eta_p^2=0.36$) and multiple comparisons (Fig. 7i). It is noteworthy that turn initiation times of all GTs robustly slowed following CNO, by an average of 1.56 s (STs: 0.62 s).

Effects of CNO on glutamate peaks during misses, cued stops and reward delivery. In contrast to turn-cue evoked maximum glutamate peaks in trials followed by turns, CNO had no effects on peak glutamate levels in GTs when the cue was not followed by a turn. In STs, however, CNO significantly reduced maximum peak levels in such trials (phenotype x treatment: ($F(1,133.99)=3.88$, $P=0.04$; Fig. 7j).

There were no effects of CNO on stop cue-locked glutamate peaks (main effects of injection and interaction: all $P>0.37$). However, and mirroring a similar finding described above (Fig. 5d), maximum peak glutamate levels were generally higher in STs (main effect of phenotype: $F(1,9.57)=5.42$, $P=0.04$; GTs: 4.79±0.73; STs: 7.33±0.8; Fig. 7k). Neither CNO nor phenotype affected glutamate maximum peaks in trials in which the stop cue was followed by false turns (main effects and interaction: all $F<1.49$, all $P>0.23$; Fig. 7l). As before (Fig. 5e), glutamate concentrations locked to reward delivery were higher in STs than in GTs (main effects of phenotype: $F(1,10.45)=22.38$, $P<0.001$, $\eta_p^2=0.68$). CNO administration to both phenotypes resulted in an extremely small decrease of glutamate peak concentrations (main effect of treatment: $F(1,412.73)=4.83$, $P=0.03$, $\eta_p^2=0.01$; interaction: $F(1,412.729)=1.35$, $P=0.25$).

Importantly, in control rats expressing the empty construct in cortico-striatal projection neurons, administration of CNO had no effect on any parameter of cue-locked glutamate peaks (main effects of treatment and interactions: all F<0.96, all *P*>0.33).

Insert Figure 8 about here

DREADD expression in prelimbic cortex predicts CNO efficacy. The efficacy of the expression of eGFP in the DMS and of mCherry in the prelimbic cortex was quantified using categories (illustrated in Fig. 8a-f). Furthermore, we computed the proportion of neurons in the prelimbic cortex in which both fluorochrome reporters were colocalized (Fig. 8h,i). As the area of eGFP expression in neuronal soma in the DMS may only partially correspond to the synaptic space of prelimbic projections, it was not unexpected that DMS eGFP transfection efficacy scores did not correlate significantly with the efficacy of CNO to reduce cued turns (GTs: R^2=0.01, *P*=0.84; STs: R^2=0.32, *P*=0.09). in contrast, in GTs, but not STs, the expression efficacy of mCherry in the prelimbic cortex, that is, of the inhibitory DREADD construct, was significantly correlated with the efficacy of CNO to attenuate cued turns (GTs: R^2=0.48, *P*=0.02; STs: R^2=0.06, *P*=0.51; Fig. 8g). Likewise, in GTs, but not STs, the proportion of neurons expressing both the reporter for the inhibitory DREADD and the retrogradely transported Cre-expressing construct was positively correlated with CNO-induced reduction of cued turns (GTs: R^2=0.77, *P*=0.0004; STs: R^2=0.06, *P*=0.51; Fig. 8j). Thus, the degree of CNO-induced inhibition of prelimbic cortex-DMS projections predicted cued turning efficacy in GTs only.

Discussion

The present experiments were designed to assess the role of cortico-striatal glutamate signaling for cued movement and movement suppression. Furthermore, by investigating rats selected for the expression of opponent cognitive-motivational biases, GTs and STs, cue-locked cortico-striatal glutamate was hypothesized to contribute to cued movements predominantly in GTs. The impact of individual differences on our findings can be illustrated by contrasting the actual results with hypothetical findings obtained had experiments been conducted in non-selected rats. 1) Turn

cue-evoked glutamate concentrations reached higher levels in GTs compared with STs. In contrast, glutamate concentrations during missed turns, stops, and locked to reward delivery, reached significantly higher levels in STs. In the absence of phenotype as a factor, cue-evoked glutamate concentrations merely would have been found to be higher during turns when compared with missed turns and stops, but not reward delivery. 2) Turn cue-evoked glutamate peak concentrations, in conjunction with single spikes, nearly doubled the likelihood for a turn in GTs relative to STs. In contrast, in conjunction with multiple glutamate spikes, relatively low glutamate peak concentrations predicted that STs were robustly more likely to turn. In the absence of phenotype as a factor, some animals would have been found to turn when peak glutamate concentrations were relatively low but multiple peaks were present, and some when the concentrations of single spikes reached the same relatively low peak concentrations (Fig. 6, left half of the upper and lower functions). Consequently, the number of glutamate spikes would have been concluded to have no impact on turn probability. 3) In GTs, but not STs, inhibition of cortico-striatal neurons reduced cued turn rates and turn cue-evoked glutamate peak concentrations, and it increased the number of glutamate peaks. In the absence of phenotype as a factor, the effects of CNO would have been found to be extremely variable, and the collective results would not have provided an interpretational framework for such a finding. 4) In GTs, but not STs, the efficacy of CNO to attenuate cued turns was significantly correlated with transcription efficacy scores for the inhibitory DREADD, and with the relative number of prelimbic-DMS neurons expressing the inhibitory DREADD. In the absence of phenotype as a factor, no such relationships would have been found (both $R^2<0.17$), limiting the attribution of limited behavioral and glutamatergic effects of DREADD activation to prelimbic cortex-DMS projections. These contrasts between actual and hypothetical results indicate the essential role of the phenotypes for the discussion of the present evidence.

Goal- and sign-tracking index the presence of larger, opponent cognitive-motivational biases (for review see Sarter and Phillips, 2018). Collectively, the evidence supports the notion that STs preferably assign motivational significance to reward cues, with the result that they perceive such cues as rewarding and worth approaching and working for. This bias by STs is illustrated by their propensity to approach and contact Pavlovian food or drug cues (e.g., Robinson and Flagel, 2009), and by the relatively greater efficacy of cocaine cues to instigate drug taking (e.g., Saunders and Robinson, 2011; Yager and Robinson, 2013). In contrast, GTs are biased toward an analysis of the behavioral utility of a reward or drug cues. While, in GTs, such cues likewise evoke an enhanced motivational state and the expectation of reward, GTs tend to not approach

and contact such cues. Such a top-down bias indexed by goal-tracking can be revealed not only by the absence of non-instrumental behavior toward reward cues. In contrast to STs, GTs were able to utilize complex occasion setters predicting the availability of cocaine (Saunders et al., 2014; Pitchers et al., 2017b). Research in humans has confirmed the presence of such broad opponent cognitive-motivational styles indexed by sign- and goal-tracking, particularly the propensity of STs to attend to cues preferably as a function of cue salience and prediction of reward (Schad et al., 2020; Duckworth et al., 2022; Colaizzi et al., 2023).

The present findings indicate that turn cue processing in the striatum of GTs is closely controlled by cortico-striatal activity, and that GTs utilize cues evoking a complex movement more reliably than STs. These findings complement prior evidence from experiments assessing the selection of cues for extended processing and behavioral control. GTs out-performed STs in tasks taxing the detection of cues, in part by deploying goal-directed attentional mechanisms to detect cues and maintain stable task performance (e.g., Paolone et al., 2013; Kucinski et al., 2018; Phillips and Sarter, 2020; Kucinski et al., 2022). The present results are consistent with a relatively less efficacious cue detection process in STs that may be mediated via deficient cortical cholinergic mechanisms (Paolone et al., 2013; Koshy Cherian et al., 2017; Pitchers et al., 2017a; Kucinski et al., 2022; Carmon et al., 2023). Consequently, subcortical mechanisms predominately contribute to behavioral control in STs (see also Flagel et al., 2011; Campus et al., 2019; Schad et al., 2020; Iglesias et al., 2023).

In GTs, inhibition of prelimbic-DMS projections attenuated cued turns and associated glutamate concentrations. In contrast, suppression of movement, as seen during cued stops, and associated glutamate release dynamics, remained unaffected by CNO and, therefore, may not depend on cortico-striatal processing of movement cues (see also Vandaele et al., 2019; Cruz et al., 2022). In GTs, turn cue-evoked glutamate concentrations as well as the presence of single peaks may be speculated to be secondary to the cue detection-mediating generation of single cholinergic transients in prelimbic cortex and resulting high-frequency oscillations (Gritton et al., 2016; Howe et al., 2017). In the DSM, single high-amplitude glutamate transients from cortical afferents may recruit multiple populations of interneurons and striatal output neurons, thereby forming, for a precise period of time, fronto-striatal cell assemblies to force cue-associated action selection (see also Hart et al., 2018a; Hart et al., 2018b; Oberto et al., 2022).

Cortico-striatal, glutamatergic terminals are also recruited, directly and indirectly via striatal interneurons, by striatal dopaminergic afferents, thereby supporting bidirectional glutamatergic-

dopaminergic interactions and allowing reward expectation and action outcome to influence the glutamatergic representation of movement cues (Bamford et al., 2004; Agnoli et al., 2013; Kosillo et al., 2016; Cai and Ford, 2018; Moss et al., 2021; Choi et al., 2023; Holly et al., 2024). Such striatal control of cortico-striatal terminals, primarily via cholinergic and dopaminergic heteroreceptors (for review see Lovinger et al., 2022), may preferentially yield suppression of action in STs. This view is consistent with several findings and considerations. 1) Glutamate concentrations in STs were relatively higher during stops, irrespective of the validity of stops (false stops or stop cue-evoked stops). 2) The presence of multiple glutamate peaks in STs (a second or third peak occurred on average 1.58±0.39 s and 1.83±0.25 s (M, SD), respectively, following cue onset), may reflect relatively slow, reverberating interactions between striatal interneurons, dopamine signaling, and cortico-striatal glutamate release (e.g., Dorst et al., 2020; Frost Nylen et al., 2021). 3) Inhibition of the prelimbic-DSM pathway impacted neither turn cue-locked glutamate release in STs nor cued stops or stop cue-locked glutamate release in either phenotype. 4) Reward delivery-locked glutamate concentrations were higher in STs than GTs. Thus, in STs, the relatively lasting glutamatergic signal of the turn cue may be speculated to primarily signal the dopaminergically-mediated expectation of reward, and also the heightened perceptual value of a reward predicting cue, that is, its incentive salience (see also Pitchers et al., 2017a; Saunders et al., 2018; Iglesias et al., 2023; Bernklau et al., 2024).

Given that CNO did not attenuate turn cue-evoked glutamate concentrations in STs, the neuronal source for striatal information about the sensory properties of the cue remains unclear. Other striatal afferent systems, originating from midbrain cholinergic and glutamatergic regions (Dautan et al., 2014; Assous et al., 2019; Dautan et al., 2020), or thalamus (Diaz-Hernandez et al., 2018), may serve as alternative sources to “import” post-perceptual cue information into striatal circuitry to support well-practiced, habitual cued action in STs and action suppression in both phenotypes.

The present results contribute to bio-behavioral conceptualizations of individual differences in the vulnerability for compulsive drug taking (e.g., Volkow et al., 2006; Robbins et al., 2012; Marhe et al., 2013; Kilts et al., 2014; George and Koob, 2017; Pitchers et al., 2018). In contrast, the significance of cognitive-motivational endophenotypic traits such as goal- and sign-tracking for neurological disorders has yet to be explored (but see Deik et al., 2012; Kucinski et al., 2018). Consistent with the view that striatal pathology contributes little to the explanation of individual, clinical severity of PD (Johansson et al., 2024), our findings predict a greater vulnerability of PD patients who preferentially utilize cortico-striatal mechanisms to process cues - that is, GTs - for cholinergic loss-associated cued movement control and falls (Sarter et al., 2014; Sarter et al.,

2021). In contrast, STs generally may be less efficient in executing cued movements, particularly in situations featuring complex and competing movement cues (e.g., Beaulne-Seguin and Nantel, 2016). As we demonstrated here, the investigation of the impact of endophenotypic indices that predict individual differences in fundamental brain function may be necessary to reveal potently predictive neuronal and cognitive markers of psychiatric and neurological disease vulnerability.

Figure Legends

Figure 1

a Distribution of PCA scores, from a total of N=378 rats (215 females) used for the analysis of CTTT performance and associated glutamatergic transients. Final phenotypic classification was based on averages from the 4th and 5th test session (rats with intermediate PCA scores, INs, are not shown). The photos on the right depict lever (CS) contact, indicative of sign-tracking behavior (top) versus CS-triggered food port entry, signifying goal-tracking behavior (bottom). The distribution of PCA scores was unaffected by sex (b) but differed among rats obtained from the two vendors (c). Relatively more rats from Inotiv were classified as STs while rats from Taconic tended to emerge relatively more often as GTs. The distribution of vendor-specific PCA scores was not affected by sex.

Figure 2

Illustration of the CTTT, trial timeline, and of a cued turn. a shows a lateral view of 1.5-m long CTTT, with Faraday shielding comprised of copper wire mesh surrounding the motor and wooden frame of the Plexiglas-lined enclosure (both grounded), 2 mounted cue lights on both ends, 1 mounted audible device centered (not visible here), and a copper reward port installed on either end of the treadmill. Web cameras were placed on each side of the treadmill for off-line analysis of the rat's performance. b Trial events and timeline. The CTTT required rats to walk on a treadmill (walking speed: 9.6 cm/s). Presentation of a turn or stop cue (tone or light for 2 s), indicated that the treadmill stopped 1 s later, and restarted after a 5-s pause, in the reverse or same direction, respectively, Successful turns and stops without turns, respectively, were rewarded by delivering a 45 mg banana pellet, on average 3.6 s following cue offset (see green square in b). c shows photographs of a cued turn, initiated within the first second of cue onset (see lines connecting the individual photos to the task timeline in b). Successive presentation of cues was separated by a variable intertrial interval (ITI) of 60±45 s during which the rat continued walking the treadmill.

Figure 3

CTTT acquisition and asymptotic performance by GTs (n=29, 13 females) and STs (n=22, 12 females). a The number of training sessions to reach CTTT criterion performance, defined as 70% correct responses to either cue for two consecutive days, neither differed between the phenotypes nor the sexes. However, baseline performance, based on data from four test sessions conducted after rats had reached criterion performance, indicated that GTs scored more cued

turns than STs (main effect of phenotype; GTs: 0.80 (M) cued turns/trials; STs: 0.73). Moreover, a main effect of day reflected that rats performed more cued turns on day 3 than on day 1 (*post hoc* Bonferroni test; b; [1]note that b and c show response ratios but ANOVAs were conducted using arcsine transformed data because ratio data violated homoscedasticity). c The relative number of cued stops did not differ between the phenotypes. There were no main effects of sex and no significant interactions between the effects of phenotype, day and sex on either measure. d Relative to the time of cue onset, GTs initiated and completed cued turns later than STs. Reflecting the parallel effects of phenotype on initiation and completion times, the actual time needed to complete turns did not differ between the phenotypes (not shown; *,**,***: $P<0.05$, 0.01, 0.001).

Figure 4

Electrochemical measurement scheme, electrode calibration, sentinel correction and glutamate peak identification. a Schematic illustration of a ceramic backbone with four platinum-iridium (Pt/Ir) recording sites, organized in two pairs, with each recording site measuring 333 µm long and 15 µm wide. The upper pair was fabricated to measure currents reflecting GLU concentration (red, also b), while the lower pair served as sentinels for background current recording and subtraction (yellow, also c). Glutamate oxidase (GO) was immobilized onto the upper (b), but not lower (c), pair of recording sites. After GO coating, a non-conducting polymer, *m*-(1,3)-phenylenediamine (*m*PD), was electroplated onto both sites to prevent the transfer of small electroactive organic molecules like dopamine to the Pt sites. Application of a 0.7 V constant potential versus an Ag/AgCl reference electrode (not shown) served to oxidize hydrogen peroxide at individual recording sites (e.g., Burmeister et al., 2000; Parikh et al., 2010b), yielding current proportional to the concentration of GLU at the recording site. d *In vitro* calibration (representative example; see Table 1 for calibration data) indicated the sensitivity, linearity of the response to increasing concentrations of glutamate, and selectivity of GO-coated recording sites (red). Sentinel sites typically did not respond to glutamate and ascorbic acid (AA) and exhibited a relatively small response to the addition of dopamine (DA) to the bath. e Electrodes were implanted into the DMS; the circles in e indicate the location of microelectrode tips in this area (red circles: placements in rats which were recorded during CTTT performance; purple circles: placements in rats in which fronto-striatal projections were silenced). f Example of a turn-cue evoked current recorded via GO-coated recording sites and, g, via sentinels. The subtracted trace is shown in h. i Glutamate trace (sentinel- and baseline-corrected) exemplifying the identification of peaks (red dots) using the PeakDet tool in Matlab. As detailed in Methods, peak identification required GLU levels above

3 SDs of pre-cue baseline levels and 1 SD (of baseline levels) above the preceding and subsequent data point.

Figure 5

GLU maximum peak concentrations locked to turn and stop cues and reward delivery. a shows representative recording traces of a GT (blue, squares) and a ST (red, triangles) during a cued turn. The time of cue onset, offset, and reward delivery are indicated by arrows, and the actual timing of the turn by horizontal bars. Identified peaks are symbolized by circles. Note that following turn cue onset, already the first subsequent data point from the GT was a peak, followed by one more peak that also constituted the maximum peak locked to the turn cue. In contrast, in the recording from the ST, only the third data point following cue onset was a peak, and it also constituted the maximum peak. Moreover, the 6th and 7th data point following cue onset were also peaks in the ST, reflecting the return to baseline GLU levels in between the first and the subsequent, turn cue-locked peaks. Reward delivery did not elicit a peak in the GT but was followed by two peaks in the ST. LMM-based analysis of GLU traces collected from N=30 rats (15 females) indicated significantly, and robustly (η_p^2=0.23) higher GLU maximum peaks in GTs following turn cues and when followed by a turn (b). In contrast, maximum GLU concentrations were higher in STs during all other response categories (missed turns, c; cued stops d; errors following stop cues were extremely rare and thus not analyzed) and following reward delivery during cued turn trials (e; b-e depict estimated marginal means (EMMs), and 95% CI; main effects of phenotype: **,***: *P*<0.01, 0.001).

Figure 6

Relative probabilities for cued turns in GTs given the presence of individual and combined properties of turn cue-evoked glutamate peaks (based on a total of 548 traces, 364 recorded during cued turns and 184 during misses, 318 from GTs and 230 from STs). The ordinate depicts relative probabilities derived from contingency table analyses. A value of 1 would indicate that GTs were as likely as STs to turn (inserted line), while a value of 2 that GTs were twice as likely as STs to turn. For each value, the associated significance level derived from contingency table analyses is indicated by the symbol color (no fill, not significant, n.s.; blue, *P*<0.05; green, *P*<0.01; magenta, *P*<0.001; red: *P*<0.0001). Regardless of other glutamate trace properties, increasing maximum peak concentrations, beginning with 2.8 µM glutamate, yielded significantly different proportions of turns and misses in GTs and STs and therefore rising relative probabilities for GTs to execute a turn ("GLU max peaks ≥x"; the slope of the linear regression of all three curves was

significantly different from zero; see Results). For example, for maximum peak concentrations ≥4 µM, GTs were 1.24 times as likely as STs to turn. The presence of a single turn cue-evoked peak, regardless of other trace properties, strongly increased the probability for GTs to turn (see Results). In conjunction with increasing amplitudes of these peaks ("1 peak only ∪ ≥x"), these probabilities did further increase, reaching, for example, 1.73 for glutamate concentrations ≥4 µM. In striking contrast, and regardless of other trace properties, the presence of 2 or 3 turn cue-evoked peaks (no more than 3 peaks were observed) significantly lowered the relative probability for a turn in GTs below 1 or, conversely, indicated that STs were 1.35 times as likely to turn as GTs (see Results). However, in conjunction with rising max amplitude threshold levels ("2 and 3 peaks ∪ max peaks ≥x"), the relative probabilities of GTs to turn increased, so that, for example, STs were only 1.17 times as likely as STs to turn at maximum peak concentrations ≥6 µM glutamate, no longer reflecting dissimilar proportions in the two phenotypes. The vertical brackets on the right symbolize significant differences between the relative probabilities of the three trace characteristics (H(3)=33.41, $P<0.0001$; Kruskal–Wallis test; multiple comparisons: *,****, $P<0.05$, 0.0001).

Figure 7

Timeline of experimental procedures and effects of CNO on CTTT performance. a: Following initial handling and screening to identify the rat's phenotype (17 GTs, 7 females; 12 STs, 6 females), rats were infused with either a Cre-dependent inhibitory DREADD or the empty control vector (both expressing mCherry; b) into the lower layers of the prelimbic cortex, and a retrogradely transported, Cre-expressing plasmid into the DMS (expressing eGFP). These rats continued to undergo CTTT performance training, followed either by (c) a test of the effects of vehicle or CNO (the blue syringes symbolizing CNO administration) or by (d) implantation of an MEA for the measurement of glutamate concentrations into the mediodorsal stratum. Following recovery from that surgery, the effects of CNO and vehicle on performance and performance-associated glutamate concentrations were assessed. In GTs, administration of CNO significantly reduced the relative number of cued turns (e), but not cued stops (f; graphs show individual data, mean and 95% CI; *post hoc* multiple comparisons: ***,****: $P<0.001$, 0.0001, Tukey's Honest Significant Difference test). CNO had no effects on cued turns or stops in rats expressing an empty control vector (not shown; see Results). In GTs, CNO administration attenuated cue-locked maximum peak glutamate concentrations during (residual) cued turns (g) and also increased the number of peaks (not shown). Residual turns took significantly more time to be initiated in GTs than STs, as was indicated by an analysis based on turn initiation times from

individual trials (h) and individual rats (the lines in i depict averaged individual turn initiation times following saline (SAL) and CNO). Note that CNO increased initiation times of residual turns in all GTs. CNO administration did not affect maximum peak glutamate concentrations in GTs during missed turns (j), cued stops (k), and false turns (l; except for I, graphs depict individual data points, EMMs, and 95% CI; multiple comparisons: *,**,***: P<0.05, 0.01, 0.001).

Figure 8

Expression of eGFP (green channel), indicating the expression of the retrograde, Cre-expressing vector, in the DMS (DMS) and, following retrograde transport, in the medial frontal cortex. The presence of the amplified mCherry fluorescent reporter signal (red channel) in cortex indicated the expression of the inhibitory hM4Di DREADD vector (see also Fig. 7b). Illustration of expression efficacy ratings for eGFP in the DMS (a,b) and of mCherry in the prelimbic cortex (prelimbic cortex; c,d), with a top score of 5 indicating complete or near-complete expression exclusively in the DMS projection field of prelimbic cortex efferent neurons (Mailly et al., 2013) and prelimbic cortex, respectively. The example of eGFP expression in the DMS in e (cc, corpus callosum) received a score of 2 (illustrated in a) because the expression field was located in part lateral to the prelimbic cortex projection field. f depicts an example of mCherry expression in the prelimbic cortex that was assigned a scores of 4 as it was restricted to the deeper layers in the prelimbic cortex and extended dorsally into cingulate cortex. In GTs, but not STs, mCherry expression scores were significantly correlated with the efficacy of CNO to reduce cued turns (g). h depicts the retrogradely transported eGFP and the expression of mCherry, including the co-expressing of both fluorochromes, primarily in layer 5 of the prelimbic cortex. The bright rectangular region in h is enlarged in i and illustrated neurons co-expressing nucleolar eGFP and cytoplasmic mCherry (white arrows). In GTs, but not STs, the proportion of double-labeled neurons in prelimbic cortex was significantly correlated with the efficacy of CNO to attenuate cued turns (j).

References

Agnoli L, Mainolfi P, Invernizzi RW, Carli M (2013) Dopamine D1-like and D2-like receptors in the dorsal striatum control different aspects of attentional performance in the five-choice serial reaction time task under a condition of increased activity of corticostriatal inputs. Neuropsychopharmacology 38:701-714.

Arnold JC, Salvatore MF (2014) Getting to compliance in forced exercise in rodents: a critical standard to evaluate exercise impact in aging-related disorders and disease. J Vis Exp 90:e51827.

Assous M, Dautan D, Tepper JM, Mena-Segovia J (2019) Pedunculopontine Glutamatergic Neurons Provide a Novel Source of Feedforward Inhibition in the Striatum by Selectively Targeting Interneurons. J Neurosci 39:4727-4737.

Avila C, Kucinski A, Sarter M (2020) Complex movement control in a rat model of Parkinsonian falls: bidirectional control by striatal cholinergic interneurons. J Neurosci 40:6049-6067.

Bakeman R (2005) Recommended effect size statistics for repeated measures designs. Behav Res Methods 37:379-384.

Balleine BW, O'Doherty JP (2010) Human and rodent homologies in action control: corticostriatal determinants of goal-directed and habitual action. Neuropsychopharmacology 35:48-69.

Bamford NS, Robinson S, Palmiter RD, Joyce JA, Moore C, Meshul CK (2004) Dopamine modulates release from corticostriatal terminals. J Neurosci 24:9541-9552.

Beaulne-Seguin Z, Nantel J (2016) Conflicting and non-conflicting visual cues lead to error in gait initiation and gait inhibition in individuals with freezing of gait. Gait Posture 49:443-447.

Bermingham KP, Doran MM, Bolger FB, Lowry JP (2022) Design optimisation and characterisation of an amperometric glutamate oxidase-based composite biosensor for neurotransmitter l-glutamic acid. Anal Chim Acta 1224:340205.

Bernklau TW, Righetti B, Mehrke LS, Jacob SN (2024) Striatal dopamine signals reflect perceived cue-action-outcome associations in mice. Nat Neurosci.

Bohnen NI, Müller MLTM, Koeppe RA, Studenski SA, Kilbourn MA, Frey KA, Albin RL (2009) History of falls in Parkinson disease is associated with reduced cholinergic activity. Neurology 73:1670-1676.

Bohnen NI, Kanel P, Zhou Z, Koeppe RA, Frey KA, Dauer WT, Albin RL, Muller M (2019) Cholinergic system changes of falls and freezing of gait in Parkinson's disease. Ann Neurol 85:538-549.

Budisantoso T, Harada H, Kamasawa N, Fukazawa Y, Shigemoto R, Matsui K (2013) Evaluation of glutamate concentration transient in the synaptic cleft of the rat calyx of Held. J Physiol 591:219-239.

Burmeister JJ, Moxon K, Gerhardt GA (2000) Ceramic-based multisite microelectrodes for electrochemical recordings. Anal Chem 72:187-192.

Cai Y, Ford CP (2018) Dopamine Cells Differentially Regulate Striatal Cholinergic Transmission across Regions through Corelease of Dopamine and Glutamate. Cell Rep 25:3148-3157 e3143.

Campus P, Covelo IR, Kim Y, Parsegian A, Kuhn BN, Lopez SA, Neumaier JF, Ferguson SM, Solberg Woods LC, Sarter M, Flagel SB (2019) The paraventricular thalamus is a critical mediator of top-down control of cue-motivated behavior in rats. Elife 8:e49041.

Carmon H, Haley EC, Parikh V, Tronson NC, Sarter M (2023) Neuro-Immune Modulation of Cholinergic Signaling in an Addiction Vulnerability Trait. eNeuro 10.

Castelhano-Carlos MJ, Baumans V (2009) The impact of light, noise, cage cleaning and in-house transport on welfare and stress of laboratory rats. Lab Anim 43:311-327.

Chatham CH, Frank MJ, Badre D (2014) Corticostriatal output gating during selection from working memory. Neuron 81:930-942.

Cheng FY, Yang YR, Wang CJ, Wu YR, Cheng SJ, Wang HC, Wang RY (2014) Factors influencing turning and its relationship with falls in individuals with Parkinson's disease. PLoS One 9:e93572.

Choi K, Piasini E, Diaz-Hernandez E, Cifuentes LV, Henderson NT, Holly EN, Subramaniyan M, Gerfen CR, Fuccillo MV (2023) Distributed processing for value-based choice by prelimbic circuits targeting anterior-posterior dorsal striatal subregions in male mice. Nat Commun 14:1920.

Clay M, Monbouquette HG (2018) A Detailed Model of Electroenzymatic Glutamate Biosensors To Aid in Sensor Optimization and in Applications in Vivo. ACS Chem Neurosci 9:241-251.

Clements JD, Lester RA, Tong G, Jahr CE, Westbrook GL (1992) The time course of glutamate in the synaptic cleft. Science 258:1498-1501.

Colaizzi JM, Flagel SB, Gearhardt AN, Borowitz MA, Kuplicki R, Zotev V, Clark G, Coronado J, Abbott T, Paulus MP (2023) The propensity to sign-track is associated with externalizing behavior and distinct patterns of reward-related brain activation in youth. Sci Rep 13:4402.

Cruz BF, Guiomar G, Soares S, Motiwala A, Machens CK, Paton JJ (2022) Action suppression reveals opponent parallel control via striatal circuits. Nature 607:521-526.

Dautan D, Huerta-Ocampo I, Witten IB, Deisseroth K, Bolam JP, Gerdjikov T, Mena-Segovia J (2014) A major external source of cholinergic innervation of the striatum and nucleus accumbens originates in the brainstem. J Neurosci 34:4509-4518.

Dautan D, Huerta-Ocampo I, Gut NK, Valencia M, Kondabolu K, Kim Y, Gerdjikov TV, Mena-Segovia J (2020) Cholinergic midbrain afferents modulate striatal circuits and shape encoding of action strategies. Nat Commun 11:1739.

Deik A, Saunders-Pullman R, San Luciano M (2012) Substances of abuse and movement disorders: complex interactions and comorbidities. Current Drug Abuse Reviews 5:243.

Devignes Q, Bordier C, Viard R, Defebvre L, Kuchcinski G, Leentjens AFG, Lopes R, Dujardin K (2022) Resting-State Functional Connectivity in Frontostriatal and Posterior Cortical Subtypes in Parkinson's Disease-Mild Cognitive Impairment. Mov Disord 37:502-512.

Diaz-Hernandez E, Contreras-Lopez R, Sanchez-Fuentes A, Rodriguez-Sibrian L, Ramirez-Jarquin JO, Tecuapetla F (2018) The Thalamostriatal Projections Contribute to the Initiation and Execution of a Sequence of Movements. Neuron 100:739-752 e735.

Dorst MC, Tokarska A, Zhou M, Lee K, Stagkourakis S, Broberger C, Masmanidis S, Silberberg G (2020) Polysynaptic inhibition between striatal cholinergic interneurons shapes their network activity patterns in a dopamine-dependent manner. Nat Commun 11:5113.

Duckworth JJ, Wright H, Christiansen P, Rose AK, Fallon N (2022) Sign-tracking modulates reward-related neural activation to reward cues, but not reward feedback. Eur J Neurosci 56:5000-5013.

Ersche KD, Barnes A, Jones PS, Morein-Zamir S, Robbins TW, Bullmore ET (2011) Abnormal structure of frontostriatal brain systems is associated with aspects of impulsivity and compulsivity in cocaine dependence. Brain 134:2013-2024.

Flagel SB, Robinson TE (2017) Neurobiological basis of individual variation in stimulus-reward learning. Current Opinion in Behavioral Sciences 13:178-185.

Flagel SB, Clark JJ, Robinson TE, Mayo L, Czuj A, Willuhn I, Akers CA, Clinton SM, Phillips PE, Akil H (2011) A selective role for dopamine in stimulus-reward learning. Nature 469:53-57.

Frost Nylen J, Carannante I, Grillner S, Hellgren Kotaleski J (2021) Reciprocal interaction between striatal cholinergic and low-threshold spiking interneurons - A computational study. Eur J Neurosci 53:2135-2148.

George O, Koob GF (2017) Individual differences in the neuropsychopathology of addiction. Dialogues Clin Neurosci 19:217-229.

Ghosh M, Yang FC, Rice SP, Hetrick V, Gonzalez AL, Siu D, Brennan EKW, John TT, Ahrens AM, Ahmed OJ (2022) Running speed and REM sleep control two distinct modes of rapid interhemispheric communication. Cell Rep 40:111028.

Gomez JL, Bonaventura J, Lesniak W, Mathews WB, Sysa-Shah P, Rodriguez LA, Ellis RJ, Richie CT, Harvey BK, Dannals RF, Pomper MG, Bonci A, Michaelides M (2017) Chemogenetics revealed: DREADD occupancy and activation via converted clozapine. Science 357:503-507.

Greenwald AG, Gonzalez R, Harris RJ, Guthrie D (1996) Effect sizes and p values: What should be reported and what should be replicated? Psychophysiology 33:175-183.

Gritton HJ, Howe WM, Mallory CS, Hetrick VL, Berke JD, Sarter M (2016) Cortical cholinergic signaling controls the detection of cues. Proc Natl Acad Sci U S A 113:E1089-1097.

Hart G, Bradfield LA, Balleine BW (2018a) Prefrontal Corticostriatal Disconnection Blocks the Acquisition of Goal-Directed Action. J Neurosci 38:1311-1322.

Hart G, Bradfield LA, Fok SY, Chieng B, Balleine BW (2018b) The Bilateral Prefronto-striatal Pathway Is Necessary for Learning New Goal-Directed Actions. Curr Biol 28:2218-2229 e2217.

Hascup KN, Hascup ER, Pomerleau F, Huettl P, Gerhardt GA (2008) Second-by-second measures of L-glutamate in the prefrontal cortex and striatum of freely moving mice. J Pharmacol Exp Ther 324:725-731.

Holly EN, Galanaugh J, Fuccillo MV (2024) Local regulation of striatal dopamine: A diversity of circuit mechanisms for a diversity of behavioral functions? Curr Opin Neurobiol 85:102839.

Howe WM, Gritton HJ, Lusk NA, Roberts EA, Hetrick VL, Berke JD, Sarter M (2017) Acetylcholine release in prefrontal cortex promotes gamma oscillations and theta-gamma coupling during cue detection. J Neurosci 37:3215-3230.

Iglesias AG, Chiu AS, Wong J, Campus P, Li F, Liu ZN, Bhatti JK, Patel SA, Deisseroth K, Akil H, Burgess CR, Flagel SB (2023) Inhibition of Dopamine Neurons Prevents Incentive Value Encoding of a Reward Cue: With Revelations from Deep Phenotyping. J Neurosci 43:7376-7392.

Jendryka M, Palchaudhuri M, Ursu D, van der Veen B, Liss B, Katzel D, Nissen W, Pekcec A (2019) Pharmacokinetic and pharmacodynamic actions of clozapine-N-oxide, clozapine, and compound 21 in DREADD-based chemogenetics in mice. Sci Rep 9:4522.

Johansson ME, Toni I, Kessels RPC, Bloem BR, Helmich RC (2024) Clinical severity in Parkinson's disease is determined by decline in cortical compensation. Brain 147:871-886.

Kilts CD, Kennedy A, Elton AL, Tripathi SP, Young J, Cisler JM, James GA (2014) Individual differences in attentional bias associated with cocaine dependence are related to varying engagement of neural processing networks. Neuropsychopharmacology 39:1135-1147.

Kim K, Muller M, Bohnen NI, Sarter M, Lustig C (2019) The cortical cholinergic system contributes to the top-down control of distraction: Evidence from patients with Parkinson's disease. Neuroimage 190:107-117.

Koopman PAR (1984) Confidence Intervals for the Ratio of Two Binomial Proportions. Biometrics 40:513-517.

Koshy Cherian A, Kucinski A, Pitchers KK, Yegla B, Parikh V, Kim Y, Valuskova P, Gurnarni S, Lindsley CW, Blakely RD, Sarter M (2017) Unresponsive choline transporter as a trait neuromarker and a causal mediator of bottom-up attentional biases. J Neurosci 37:2947-2959.

Kosillo P, Zhang YF, Threlfell S, Cragg SJ (2016) Cortical Control of Striatal Dopamine Transmission via Striatal Cholinergic Interneurons. Cereb Cortex 26:4160-4169.

Kucinski A, Lustig C, Sarter M (2018) Addiction vulnerability trait impacts complex movement control: Evidence from sign-trackers. Behav Brain Res 350:139-148.

Kucinski A, Avila C, Sarter M (2022) Basal Forebrain Chemogenetic Inhibition Converts the Attentional Control Mode of Goal-Trackers to That of Sign-Trackers. eNeuro 9:Eneuro.0418-0422.2022.

Kucinski A, Albin RL, Lustig C, Sarter M (2015) Modeling falls in Parkinson's disease: Slow gait, freezing episodes and falls in rats with extensive striatal dopamine loss. Behav Brain Res 282:155-164.

Kucinski A, Paolone G, Bradshaw M, Albin R, Sarter M (2013) Modeling fall propensity in Parkinson's disease: Deficits in the attentional control of complex movements in rats with cortical-cholinergic and striatal-dopaminergic deafferentation. J Neurosci 33:16522-16539.

Lawson KA, Ruiz CM, Mahler SV (2023) A head-to-head comparison of two DREADD agonists for suppressing operant behavior in rats via VTA dopamine neuron inhibition. Psychopharmacology (Berl) 240:2101-2110.

Lovinger DM, Mateo Y, Johnson KA, Engi SA, Antonazzo M, Cheer JF (2022) Local modulation by presynaptic receptors controls neuronal communication and behaviour. Nat Rev Neurosci 23:191-203.

Mahler SV, Aston-Jones G (2018) CNO Evil? Considerations for the Use of DREADDs in Behavioral Neuroscience. Neuropsychopharmacology 43:934-936.

Mailly P, Aliane V, Groenewegen HJ, Haber SN, Deniau JM (2013) The rat prefrontostriatal system analyzed in 3D: evidence for multiple interacting functional units. J Neurosci 33:5718-5727.

Marhe R, Luijten M, van de Wetering BJ, Smits M, Franken IH (2013) Individual differences in anterior cingulate activation associated with attentional bias predict cocaine use after treatment. Neuropsychopharmacology 38:1085-1093.

Marshall AT, Ostlund SB (2018) Repeated cocaine exposure dysregulates cognitive control over cue-evoked reward-seeking behavior during Pavlovian-to-instrumental transfer. Learn Mem 25:399-409.

Martinez V, Sarter M (2008) Detection of the moderately beneficial cognitive effects of low-dose treatment with haloperidol or clozapine in an animal model of the attentional impairments of schizophrenia. Neuropsychopharmacology 33:2635-2647.

Matthews EA, Sun W, McMahon SM, Doengi M, Halka L, Anders S, Muller JA, Steinlein P, Vana NS, van Dyk G, Pitsch J, Becker AJ, Pfeifer A, Kavalali ET, Lamprecht A, Henneberger C, Stein V, Schoch S, Dietrich D (2022) Optical analysis of glutamate spread in the neuropil. Cereb Cortex 32:3669-3689.

Mattinson CE, Burmeister JJ, Quintero JE, Pomerleau F, Huettl P, Gerhardt GA (2011) Tonic and phasic release of glutamate and acetylcholine neurotransmission in sub-regions of the rat prefrontal cortex using enzyme-based microelectrode arrays. J Neurosci Methods 202:199-208.

Mendonca PRF, Tagliatti E, Langley H, Kotzadimitriou D, Zamora-Chimal CG, Timofeeva Y, Volynski KE (2022) Asynchronous glutamate release is enhanced in low release efficacy synapses and dispersed across the active zone. Nat Commun 13:3497.

Meyer PJ, Lovic V, Saunders BT, Yager LM, Flagel SB, Morrow JD, Robinson TE (2012) Quantifying individual variation in the propensity to attribute incentive salience to reward cues. PLoS One 7:e38987.

Michel MC, Murphy TJ, Motulsky HJ (2020) New Author Guidelines for Displaying Data and Reporting Data Analysis and Statistical Methods in Experimental Biology. Mol Pharmacol 97:49-60.

Mitchell KM (2004) Acetylcholine and choline amperometric enzyme sensors characterized in vitro and in vivo. Anal Chem 76:1098-1106.

Moss MM, Zatka-Haas P, Harris KD, Carandini M, Lak A (2021) Dopamine Axons in Dorsal Striatum Encode Contralateral Visual Stimuli and Choices. J Neurosci 41:7197-7205.

Motulsky H (2018) Intuitive biostatistics. New York: Oxford University Press.

North AJ (2006) Seeing is believing? A beginners' guide to practical pitfalls in image acquisition. J Cell Biol 172:9-18.

Oberto VJ, Boucly CJ, Gao H, Todorova R, Zugaro MB, Wiener SI (2022) Distributed cell assemblies spanning prefrontal cortex and striatum. Curr Biol 32:1-13 e16.

Paolone G, Angelakos CC, Meyer PJ, Robinson TE, Sarter M (2013) Cholinergic control over attention in rats prone to attribute incentive salience to reward cues. J Neurosci 33:8321-8335.

Parikh V, Kozak R, Martinez V, Sarter M (2007a) Prefrontal Acetylcholine Release Controls Cue Detection on Multiple Timescales. Neuron 56:141-154.

Parikh V, Kozak R, Martinez V, Sarter M (2007b) Prefrontal acetylcholine release controls cue detection on multiple timescales. Neuron 56:141-154.

Parikh V, Man K, Decker MW, Sarter M (2008) Glutamatergic contributions to nicotinic acetylcholine receptor agonist-evoked cholinergic transients in the prefrontal cortex. J Neurosci 28:3769-3780.

Parikh V, Ji J, Decker MW, Sarter M (2010a) Prefrontal β2 Subunit-Containing and α7 Nicotinic Acetylcholine Receptors Differentially Control Glutamatergic and Cholinergic Signaling. The Journal of Neuroscience 30:3518-3530.

Parikh V, Ji J, Decker MW, Sarter M (2010b) Prefrontal beta2 subunit-containing and alpha7 nicotinic acetylcholine receptors differentially control glutamatergic and cholinergic signaling. J Neurosci 30:3518-3530.

Parikh V, Naughton SX, Shi X, Kelley LK, Yegla B, Tallarida CS, Rawls SM, Unterwald EM (2014) Cocaine-induced neuroadaptations in the dorsal striatum: glutamate dynamics and behavioral sensitization. Neurochem Int 75:54-65.

Phillips KB, Sarter M (2020) Addiction vulnerability and the processing of significant cues: Sign-, but not goal-, tracker perceptual sensitivity relies on cue salience. Behav Neurosci 134:133-143.

Pitchers KK, Sarter M, Robinson TE (2018) The hot 'n' cold of cue-induced drug relapse. Learn Mem 25:474-480.

Pitchers KK, Kane LF, Kim Y, Robinson TE, Sarter M (2017a) 'Hot' vs. 'cold' behavioural-cognitive styles: motivational-dopaminergic vs. cognitive-cholinergic processing of a Pavlovian cocaine cue in sign- and goal-tracking rats. Eur J Neurosci 46:2768-2781.

Pitchers KK, Phillips KB, Jones JL, Robinson TE, Sarter M (2017b) Diverse Roads to Relapse: A Discriminative Cue Signaling Cocaine Availability Is More Effective in Renewing Cocaine Seeking in Goal Trackers Than Sign Trackers and Depends on Basal Forebrain Cholinergic Activity. Journal of Neuroscience 37:7198-7208.

Pitchers KK, Flagel SB, O'Donnell EG, Woods LC, Sarter M, Robinson TE (2015) Individual variation in the propensity to attribute incentive salience to a food cue: influence of sex. Behav Brain Res 278:462-469.

Posner MI, Snyder CR, Davidson BJ (1980) Attention and the detection of signals. J Exp Psychol 109:160-174.

Postuma RB, Dagher A (2006) Basal ganglia functional connectivity based on a meta-analysis of 126 positron emission tomography and functional magnetic resonance imaging publications. Cereb Cortex 16:1508-1521.

Quintero JE, Pomerleau F, Huettl P, Johnson KW, Offord J, Gerhardt GA (2011) Methodology for rapid measures of glutamate release in rat brain slices using ceramic-based

microelectrode arrays: Basic characterization and drug pharmacology. Brain Research 1401:1-9.

Rasooli A, Zivari Adab H, Chalavi S, Monteiro TS, Dhollander T, Mantini D, Swinnen SP (2021) Prefronto-Striatal Structural Connectivity Mediates Adult Age Differences in Action Selection. J Neurosci 41:331-341.

Robbins TW, Gillan CM, Smith DG, de Wit S, Ersche KD (2012) Neurocognitive endophenotypes of impulsivity and compulsivity: towards dimensional psychiatry. Trends Cogn Sci 16:81-91.

Robinson TE, Flagel SB (2009) Dissociating the predictive and incentive motivational properties of reward-related cues through the study of individual differences. Biol Psychiatry 65:869-873.

Rochester L, Yarnall AJ, Baker MR, David RV, Lord S, Galna B, Burn DJ (2012) Cholinergic dysfunction contributes to gait disturbance in early Parkinson's disease. Brain 135:2779-2788.

Rusakov DA, Kullmann DM (1998) Extrasynaptic glutamate diffusion in the hippocampus: ultrastructural constraints, uptake, and receptor activation. J Neurosci 18:3158-3170.

Rutherford EC, Pomerleau F, Huettl P, Strömberg I, Gerhardt GA (2007) Chronic second-by-second measures of L-glutamate in the central nervous system of freely moving rats. J Neurochem 102:712-722.

Sarter M, Fritschy JM (2008) Reporting statistical methods and statistical results in EJN. Eur J Neurosci 28:2363-2364.

Sarter M, Phillips KB (2018) The neuroscience of cognitive-motivational styles: Sign- and goal-trackers as animal models. Behav Neurosci 132:1-12.

Sarter M, Albin RL, Kucinski A, Lustig C (2014) Where attention falls: Increased risk of falls from the converging impact of cortical cholinergic and midbrain dopamine loss on striatal function. Exp Neurol 257:120-129.

Sarter M, Avila C, Kucinski A, Donovan E (2021) Make a Left Turn: Cortico-Striatal Circuitry Mediating the Attentional Control of Complex Movements. Mov Disord 36:535-546.

Saunders BT, Robinson TE (2010) A cocaine cue acts as an incentive stimulus in some but not others: implications for addiction. Biol Psychiatry 67:730-736.

Saunders BT, Robinson TE (2011) Individual variation in the motivational properties of cocaine. Neuropsychopharmacology 36:1668-1676.

Saunders BT, O'Donnell EG, Aurbach EL, Robinson TE (2014) A cocaine context renews drug seeking preferentially in a subset of individuals. Neuropsychopharmacology 39:2816-2823.

Saunders BT, Richard JM, Margolis EB, Janak PH (2018) Dopamine neurons create Pavlovian conditioned stimuli with circuit-defined motivational properties. Nat Neurosci 21:1072-1083.

Schad DJ, Rapp MA, Garbusow M, Nebe S, Sebold M, Obst E, Sommer C, Deserno L, Rabovsky M, Friedel E, Romanczuk-Seiferth N, Wittchen HU, Zimmermann US, Walter H, Sterzer P, Smolka MN, Schlagenhauf F, Heinz A, Dayan P, Huys QJM (2020) Dissociating neural learning signals in human sign- and goal-trackers. Nat Hum Behav 4:201-214.

Schielzeth H, Dingemanse NJ, Nakagawa S, Westneat DF, Allegue H, Teplitsky C, Réale D, Dochtermann NA, Garamszegi LZ, Araya-Ajoy YG, Sutherland C (2020) Robustness of linear mixed-effects models to violations of distributional assumptions. Methods Ecol Evol 11:1141-1152.

Sharpe MJ, Stalnaker T, Schuck NW, Killcross S, Schoenbaum G, Niv Y (2019) An Integrated Model of Action Selection: Distinct Modes of Cortical Control of Striatal Decision Making. Annu Rev Psychol 70:53-76.

Shepherd GM (2013) Corticostriatal connectivity and its role in disease. Nat Rev Neurosci 14:278-291.

Sherafat Y, Bautista M, Fowler JP, Chen E, Ahmed A, Fowler CD (2020) The Interpeduncular-Ventral Hippocampus Pathway Mediates Active Stress Coping and Natural Reward. eNeuro 7.

Stack E, Ashburn A (2008) Dysfunctional turning in Parkinson's disease. Disabil Rehabil 30:1222-1229.

Tritsch NX, Sabatini BL (2012) Dopaminergic modulation of synaptic transmission in cortex and striatum. Neuron 76:33-50.

Turner JG, Parrish JL, Hughes LF, Toth LA, Caspary DM (2005) Hearing in laboratory animals: strain differences and nonauditory effects of noise. Comp Med 55:12-23.

van Schouwenburg MR, O'Shea J, Mars RB, Rushworth MF, Cools R (2012) Controlling human striatal cognitive function via the frontal cortex. J Neurosci 32:5631-5637.

Vandaele Y, Mahajan NR, Ottenheimer DJ, Richard JM, Mysore SP, Janak PH (2019) Distinct recruitment of dorsomedial and dorsolateral striatum erodes with extended training. Elife 8.

Verbeke G, Molenberghs G (2009) Linear mixed models for longitudinal data. New York: Springer.

Volkow ND, Wang GJ, Telang F, Fowler JS, Logan J, Childress AR, Jayne M, Ma Y, Wong C (2006) Cocaine cues and dopamine in dorsal striatum: mechanism of craving in cocaine addiction. J Neurosci 26:6583-6588.

Yager LM, Robinson TE (2010) Cue-induced reinstatement of food seeking in rats that differ in their propensity to attribute incentive salience to food cues. Behav Brain Res 214:30-34.

Yager LM, Robinson TE (2013) A classically conditioned cocaine cue acquires greater control over motivated behavior in rats prone to attribute incentive salience to a food cue. Psychopharmacology (Berl) 226:217-228.

Yager LM, Pitchers KK, Flagel SB, Robinson TE (2015) Individual variation in the motivational and neurobiological effects of an opioid cue. Neuropsychopharmacology 40:1269-1277.

Yarnall A, Rochester L, Burn DJ (2011) The interplay of cholinergic function, attention, and falls in Parkinson's disease. Mov Disord 26:2496-2503.

Yu Z, Guindani M, Grieco SF, Chen L, Holmes TC, Xu X (2022) Beyond t test and ANOVA: applications of mixed-effects models for more rigorous statistical analysis in neuroscience research. Neuron 110:21-35.

Table 1. Electrode *in vitro* calibration characteristics

	Sensitivity (Slope) to Glutamate	Selectivity for Glutamate over Ascorbic Acid (AA)	Limit of Detection of Glutamate	Linearity of Response (R^2)
Minimum Criteria	>5 pA/μM	>50:1 glutamate:AA	<1.0 μM	R^2 >0.95
Measured (N=30; M±SEM):	11.52±0.10	132.08±2.41	0.31±0.01	0.99±0.001

Figure 1

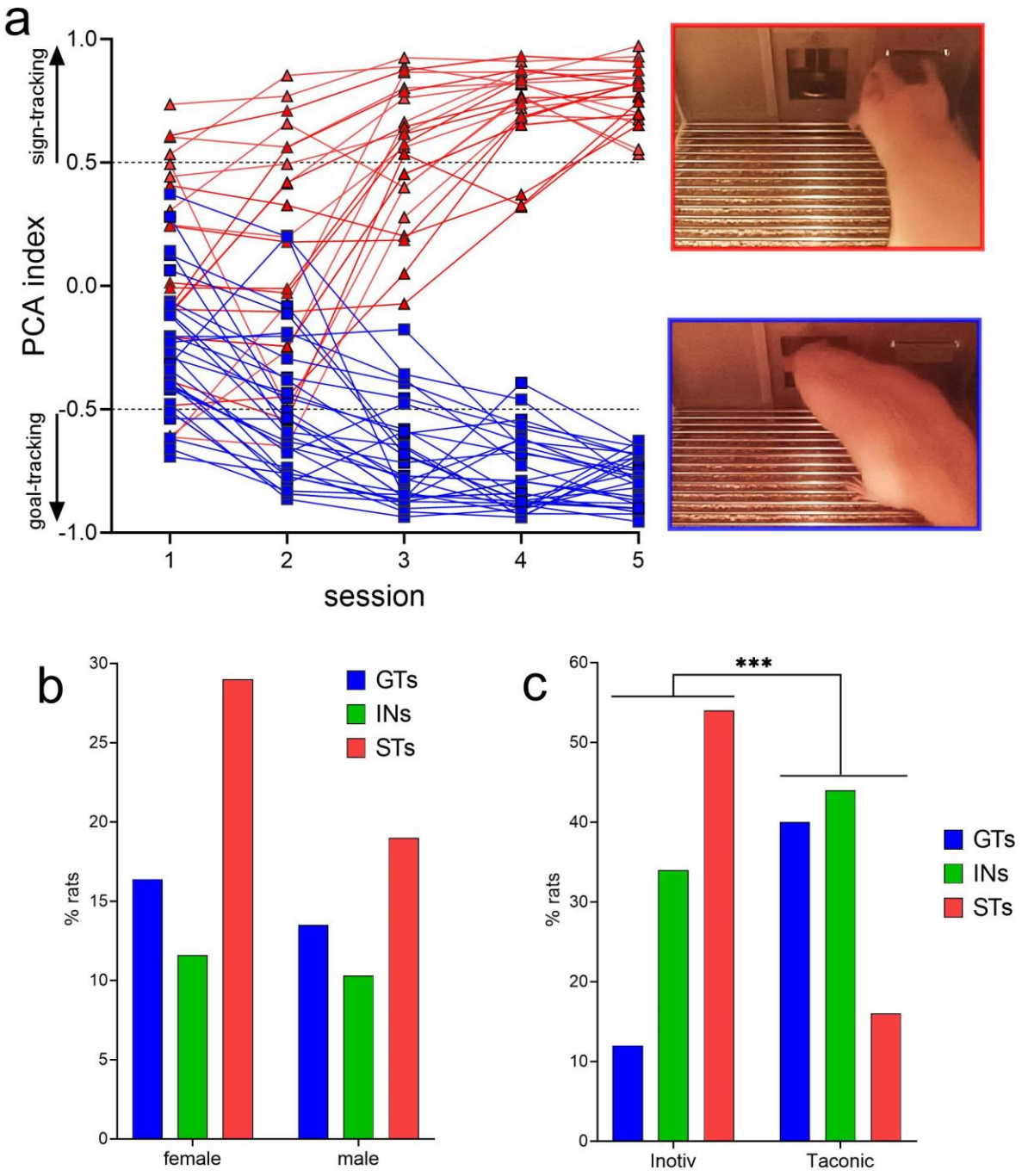
a
sign-tracking
goal-tracking
PCA index
1.0
0.5
0.0
-0.5
-1.0
1
2
3
4
5
session
b
GTs
INs
STs
% rats
30
25
20
15
10
5
0
female
male
c
***
GTs
INs
STs
% rats
60
50
40
30
20
10
0
Inotiv
Taconic

Figure 2

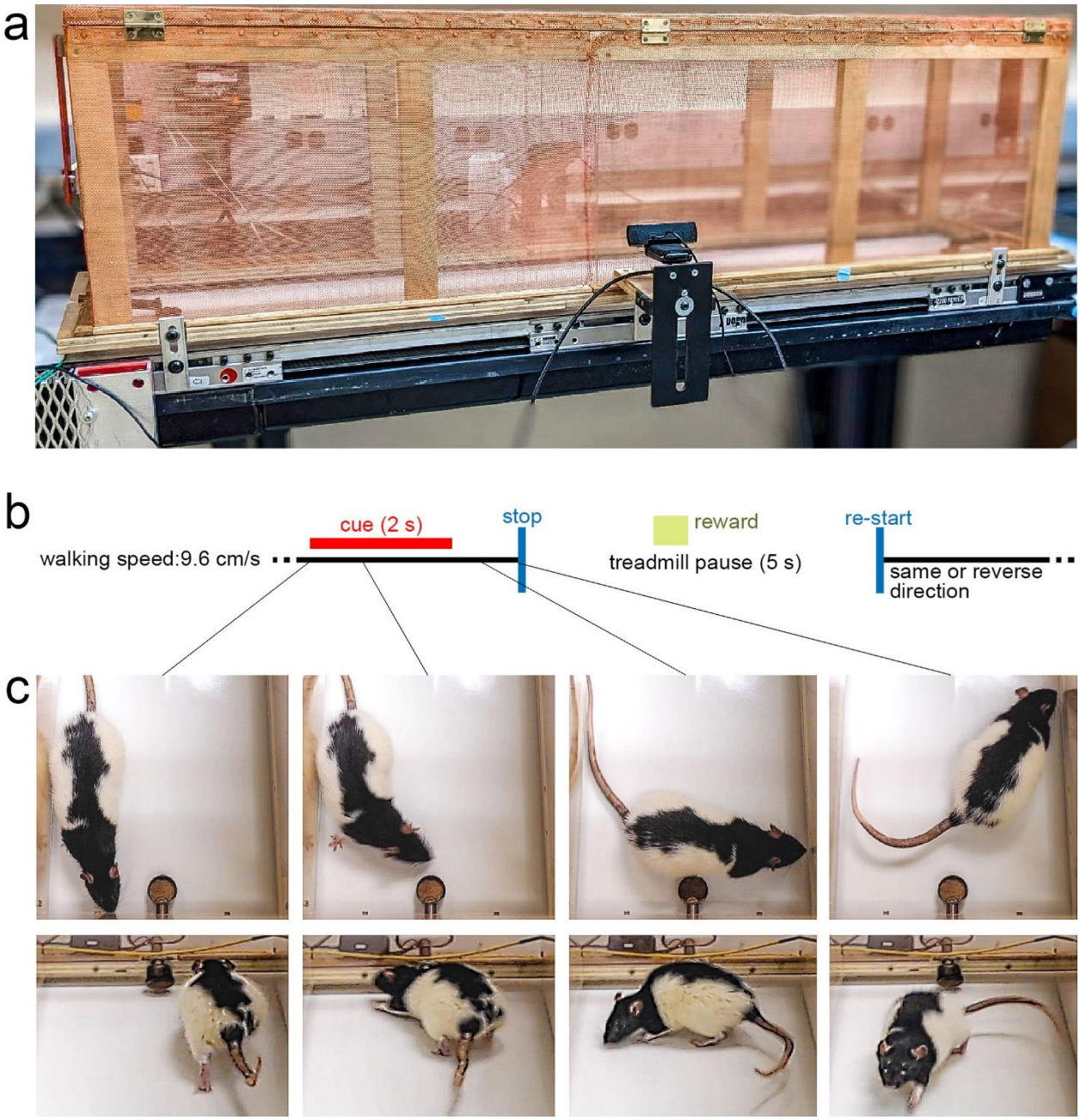
a
b
cue (2 s)
stop
reward
re-start
walking speed:9.6 cm/s
treadmill pause (5 s)
same or reverse direction
c

Figure 3

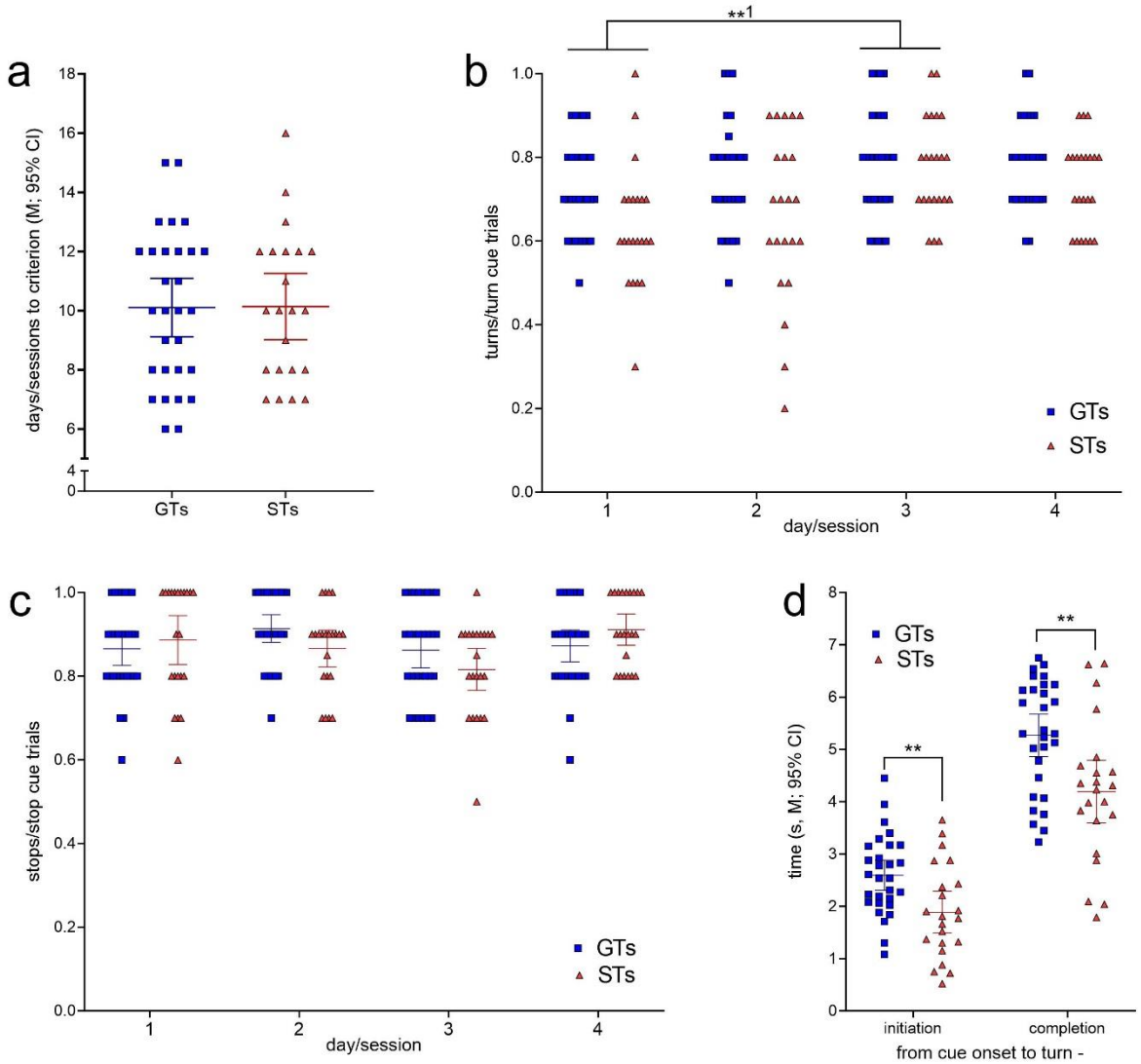
a
days/sessions to criterion (M; 95% CI)
GTs
STs
b
**1
turns/turn cue trials
day/session
GTs
STs
c
stops/stop cue trials
day/session
GTs
STs
d
time (s, M; 95% CI)
**
**
initiation
completion
from cue onset to turn -
GTs
STs

Figure 4

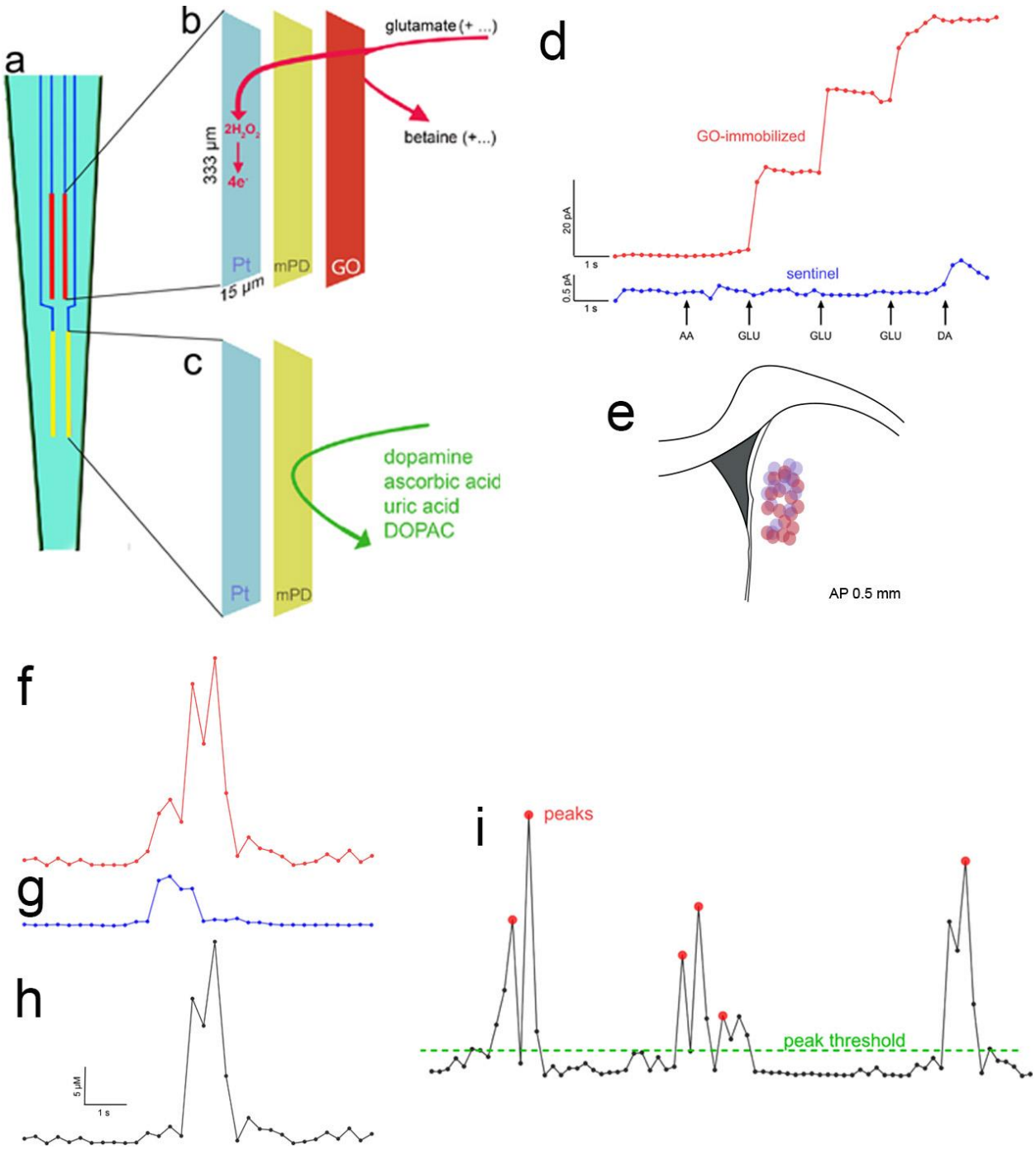
a
b
glutamate (+ ...)
betaine (+...)
333 µm
2H2O2
4e-
Pt
mPD
GO
15 µm
c
dopamine
ascorbic acid
uric acid
DOPAC
Pt
mPD
d
GO-immobilized
20 pA
1 s
sentinel
0.5 pA
1 s
AA
GLU
GLU
GLU
DA
e
AP 0.5 mm
f
g
h
5 µM
1 s
i
peaks
peak threshold

Figure 5

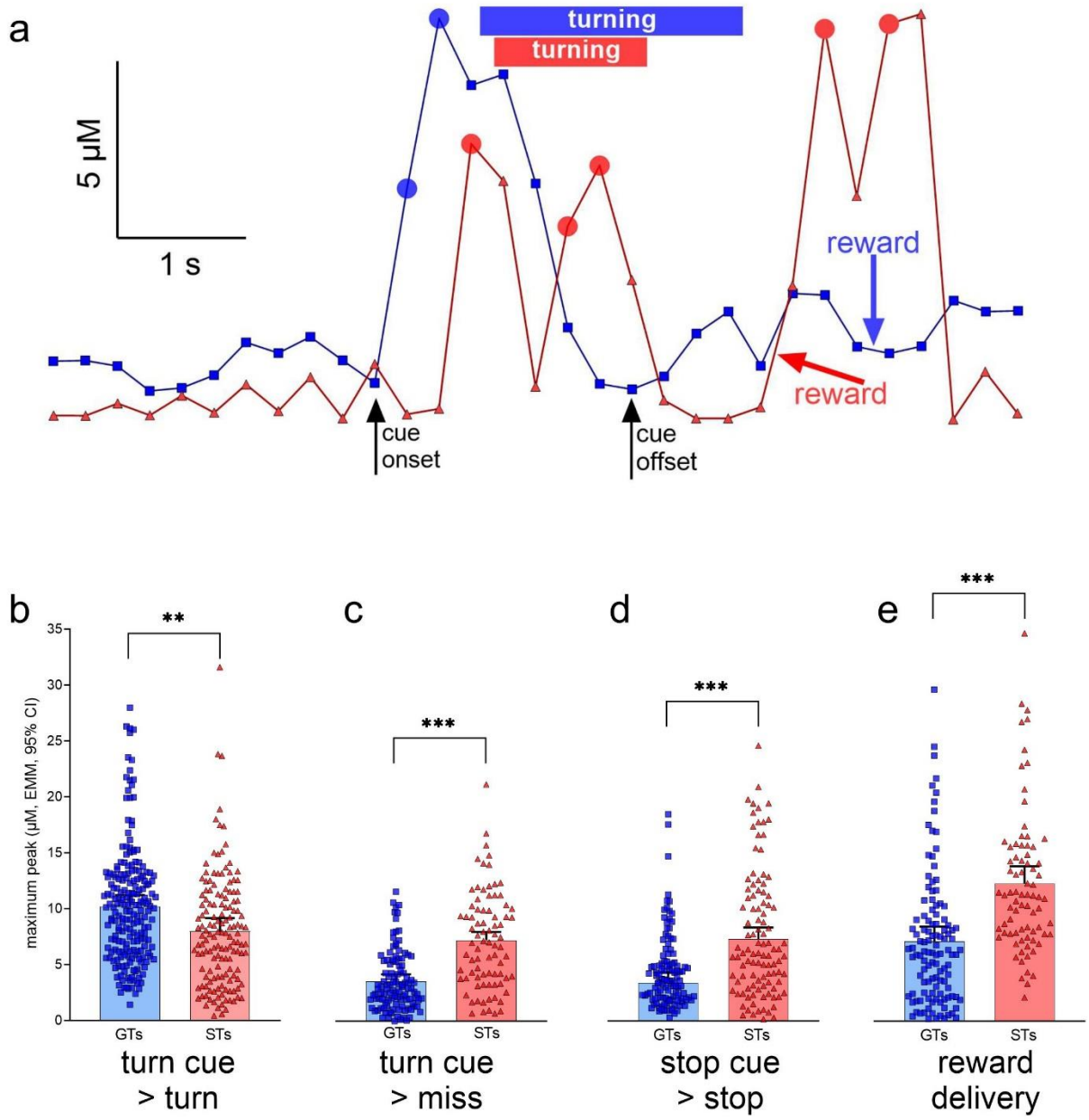
a
turning
turning
5 µM
1 s
reward
reward
cue
onset
cue
offset
b
c
d
e
maximum peak (µM, EMM, 95% CI)
**
***
***
***
GTs
STs
turn cue
> turn
turn cue
> miss
stop cue
> stop
reward
delivery

Figure 6

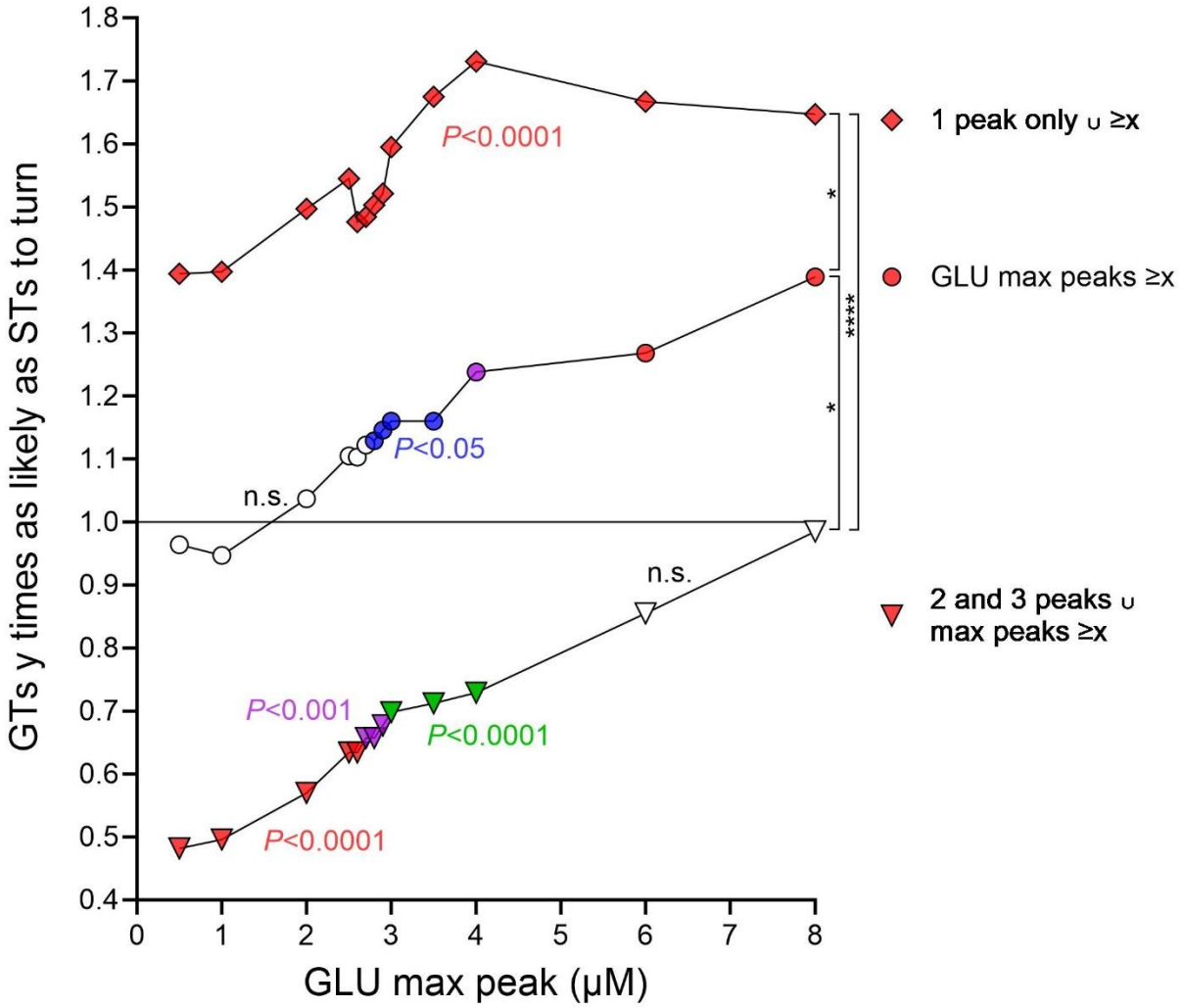
GTs y times as likely as STs to turn
GLU max peak (μM)
1 peak only ∪ ≥x
GLU max peaks ≥x
2 and 3 peaks ∪ max peaks ≥x
P<0.0001
P<0.05
n.s.
P<0.001
P<0.0001
P<0.0001
n.s.
*
*
****

Figure 7

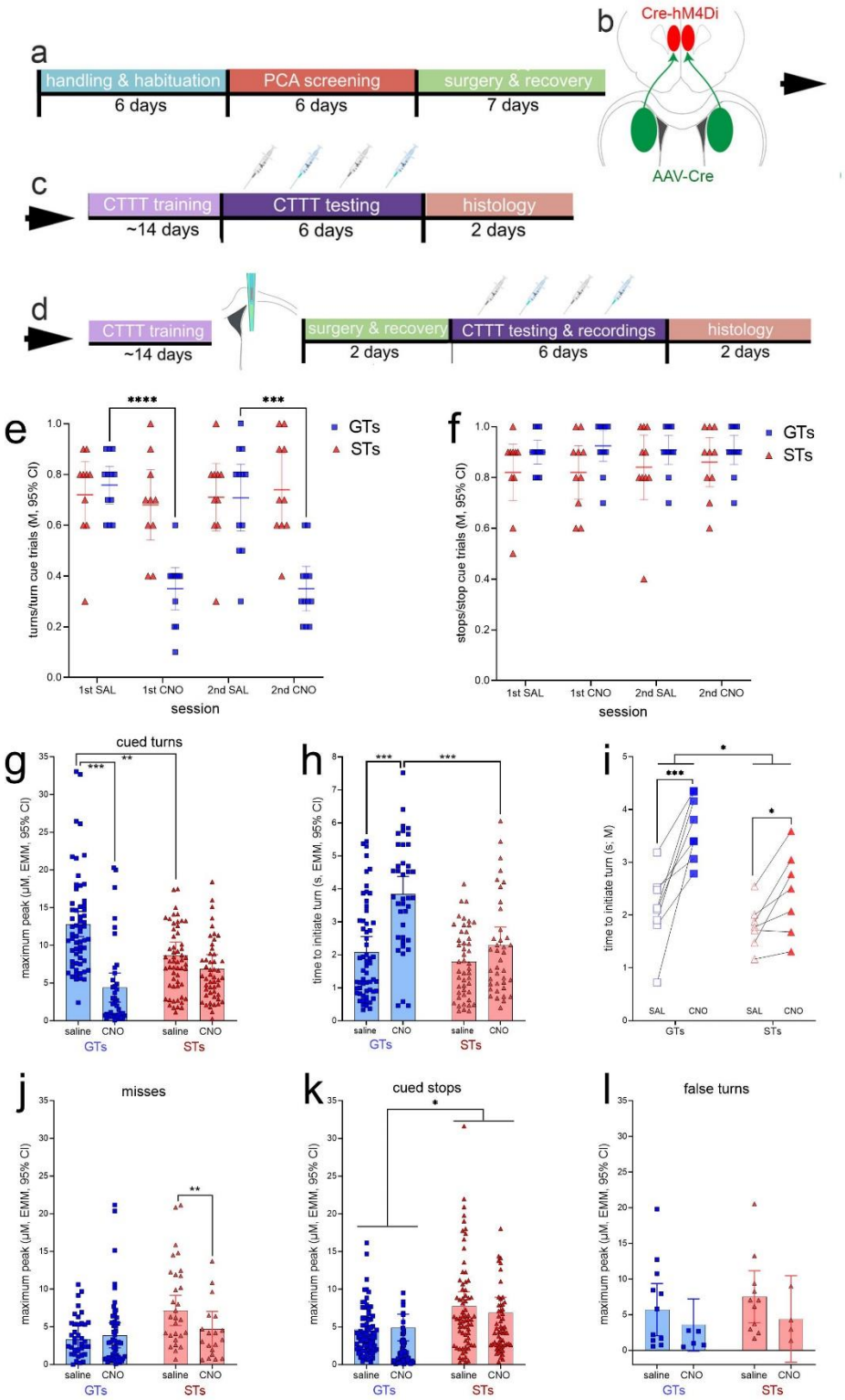
a
handling & habituation
6 days
PCA screening
6 days
surgery & recovery
7 days
b
Cre-hM4Di
AAV-Cre
c
CTTT training
~14 days
CTTT testing
6 days
histology
2 days
d
CTTT training
~14 days
surgery & recovery
2 days
CTTT testing & recordings
6 days
histology
2 days
e
turns/turn cue trials (M, 95% CI)
GTs
STs
1st SAL
1st CNO
2nd SAL
2nd CNO
session
f
stops/stop cue trials (M, 95% CI)
session
g
cued turns
maximum peak (µM, EMM, 95% CI)
saline
CNO
GTs
STs
h
time to initiate turn (s, EMM, 95% CI)
i
time to initiate turn (s, M)
SAL
CNO
j
misses
k
cued stops
l
false turns

Figure 8

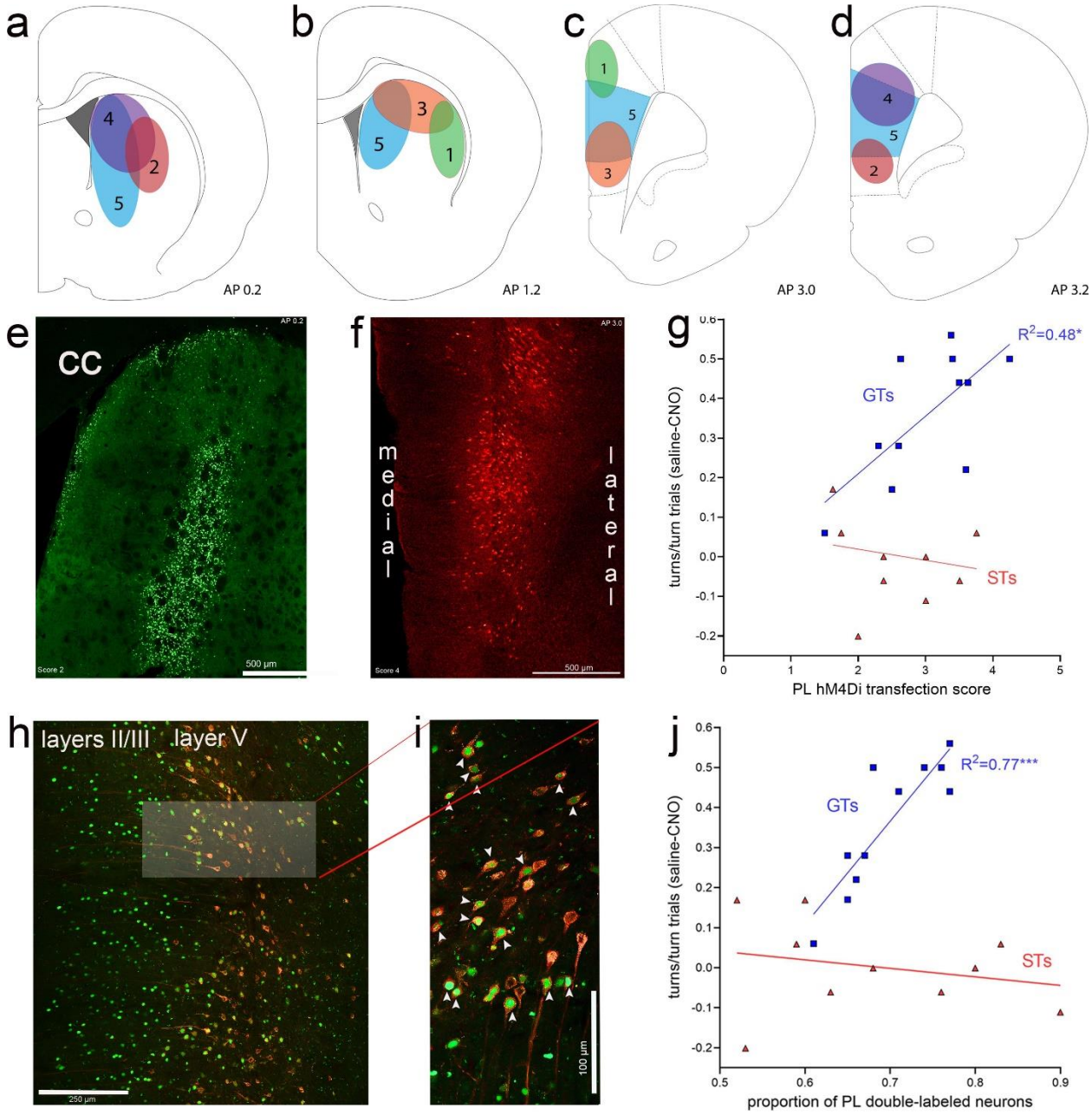
a
b
c
d
AP 0.2
AP 1.2
AP 3.0
AP 3.2
e
cc
f
medial
lateral
g
R2=0.48*
GTs
STs
turns/turn trials (saline-CNO)
PL hM4Di transfection score
h
layers II/III
layer V
i
j
R2=0.77***
GTs
STs
turns/turn trials (saline-CNO)
proportion of PL double-labeled neurons